Pre-publication version
K.C. Leong et al. Applied Thermal Engineering 112 (2017) 999–1019
http://dx.doi.org/10.1016/j.applthermaleng.2016.10.138

A critical review of pool and flow boiling heat transfer of dielectric fluids on enhanced surfaces

K.C. Leong*, J.Y. Ho, K.K. Wong
Singapore Centre for 3D Printing, School of Mechanical and Aerospace Engineering, Nanyang Technological University, 50 *Nanyang Avenue, Singapore* 639798, *Republic of Singapore*

ABSTRACT

Pool and flow boiling of dielectric fluids are efficient direct liquid cooling techniques with immense potential in the thermal management of electronic/electrical components. However, due to the increasing demand for higher rate of heat flux dissipation, many enhanced surfaces have been developed to further augment the boiling performance of dielectric fluids. This has resulted in large collections of experimental data and predictive models being reported in the recent years. The present review seeks to consolidate and highlight the recent developments in pool and flow boiling of dielectric fluids with enhanced surfaces. The various models developed to characterize the nucleate boiling curves and to predict critical heat fluxes of plain and enhanced surface are critically examined. The effects of enhanced surfaces on the bubble dynamics in dielectric fluids are also examined and the fundamental studies on boiling found in the recent literature are provided. In addition, attempts are made to categorize the various enhanced surfaces based on their fabrication techniques and their heat transfer performances and to elucidate the thermal transport mechanisms involved. Based on the literature surveyed, the various experimental results are compared, existing shortfalls are identified and areas which require further investigations are proposed.

KEYWORDS: Heat transfer; pool boiling; flow boiling; dielectric fluids; enhanced surfaces

1. Introduction

The advent in nanotechnology along with the continuous miniaturization of electronics and increasing transistor packing densities have resulted in the exponential increase in chip-level heat flux. It was projected that heat dissipated from the microprocessor could reach 200 W/cm^2 to 300 W/cm^2 and in some cases, on-chip hot spot heat fluxes as high as 1.5 kW/cm^2 were reported [1]. Due to this increase, efficient thermal management solutions are crucial to maintain the electronic devices within the operating temperature limits. Pool and flow boiling are direct liquid cooling techniques which have demonstrated significantly higher heat transfer performance as compared to single-phase cooling schemes [2, 3]. These cooling techniques involve phase change in the thermal transport process and reduce the interfacial resistance otherwise present in indirect cooling. Due to their immense cooling potential without the need for elaborate operating facilities, pool and flow boiling have been employed in the cooling of high heat flux electronic and electrical devices such as high performance electronic computers [4], batteries in electric vehicles [5] and avionics components [6]. As the coolant fluids are in direct contact with the electronic heat sources, dielectric fluids such as fluorocarbon fluids (FC-72, FC-87 and PF-5060) and hydrofluoroethers (HFE-7000, HFE-7100, HFE-7300) are often the fluids of choice due to their chemical compatibility, electrical inertness and high dielectric strength. In addition, due to their low boiling points, dielectric fluids are also highly desirable for boiling heat transfer applications to preserve the die temperatures within the recommended range of 80ºC to 130ºC [1]. However, the low surface tension and high-wetting nature of these

* Corresponding author
E-mail address: mkcleong@ntu.edu.sg (K.C. Leong)

fluids which enable the fluids to penetrate deep into the cavity sites, have resulted in noticeably higher incipient superheats as compared to conventional fluids such as water [7]. As shown in Table 1, their thermophysical properties such as latent heat of vaporization and liquid specific heat are also poorer than those of water.

Nomenclature

A	area (m^2)
A_v	area of vapor stem (m^2)
A_w	area of wall (m^2)
C_{pl}	liquid specific heat (J/kg·K)
D	channel diameter (m)
D_b	bubble diameter at departure (m)
f	bubble departure frequency (s^{-1})
g	acceleration of gravity (m/s^2)
G	mass velocity ($kg/m^2 \cdot s$)
h	heat transfer coefficient ($W/m^2 \cdot K$)
h_{fg}	latent heat of vaporization (kJ/kg)
k	thermal conductivity (W/m·K)
K	ratio of area of influence of bubble to cross-sectional area of bubble
L	length of heater (m)
L^*	non-dimensional characteristic length $(L(g(\rho_l - \rho_g)/\sigma)^{1/2})$
N	nucleation site density
q	heat rate (W)
q''	heat flux (W/m^2)
r	surface roughness factor
S	thermal active parameter $(\delta(\rho C_p k)^{1/2})$
T	temperature (°C)
$\bar{V}_{ME}$	volume of microlayer evaporated (m^3)

Greek Symbols

σ	surface tension (N/m)
ρ	density (kg/m^3)
β	contact angle (°)
ϕ	surface orientation (°)
φ_s	void fraction
μ	dynamic viscosity (kg/m·s)
υ	kinematic viscosity (m^2/s)
γ	fluid's thermal expansion coefficient (K^{-1})
α	thermal diffusivity (m^2/s)
ε	porosity
δ	thickness (m)

Subscripts

ave	average
b	boiling
g	vapor
l	fluid
nc	natural convection
sat	saturated
sub	subcooled
t	total
w	wall
∞	bulk fluid
ME	microlayer evaporation

Constants

C_{sf}	constant in Eq. (1)
n	constant in Eq. (1)
s	constant in Eq. (1)
A_1	constant in Eq. (8)
A_2	constant in Eq. (8)

Dimensionless numbers

Bl	Boiling number
Bo	Bond number
Co	Confinement number
Fe	Froude number
Pr	Prandtl number
Re	Reynolds number
We	Weber number

To overcome these drawbacks, many surface modification techniques with the aim of enhancing boiling heat transfer with dielectric fluids have been developed and extensively investigated. Direct coating methods such as electrochemical deposition, chemical vapor deposition and direct powder sintering have been studied and remarkable enhancements in boiling heat transfer coefficients and critical heat fluxes were reported. On the other hand, intrinsic surface features developed using MEMS/NEMS technologies, CNC machining, additive manufacturing (AM) and other advanced manufacturing techniques have also achieved significant boiling heat transfer augmentation. Recently, there are several review articles on boiling heat transfer. Ciloglu and Bolukbasi [8] presented the potential heat transfer applications of nanofluids and provided a detailed survey of existing pool boiling results with nanofluids. Subsequently, a review on flow boiling heat transfer with nanofluids was undertaken by Fang et al. [9]. On the other hand, various porous surface fabrication techniques for enhancing pool boiling were reviewed by Patil and Kandlikar [10] and more recently, Shojaeian and Kosar [11] and Kim et al. [12] presented comprehensive data of pool and flow boiling with micro- and nanostructured surfaces. References [10 – 12] focus mainly on the surface modification techniques for enhancing boiling.

In this paper, recent developments in augmenting pool and flow boiling heat transfer of dielectric fluids with enhanced surfaces are critically reviewed. The various methods employed to fabricate these surfaces and their levels of enhancements are elaborated. The effects of enhanced surfaces on the bubble dynamics in dielectric fluids are examined and the fundamental studies on boiling found in recent literature are also provided. Based on the literature surveyed, existing shortfalls and areas which require further investigations are identified.

2. Pool boiling

2.1 Overview

The Nukiyama boiling curve [14] (Fig. 1) which relates the heat flux dissipated from the heated surface to its wall superheat is typically observed in most boiling processes and can be classified into four distinct regimes, namely, natural convection, nucleate boiling, transition boiling and film boiling. For practical applications, it is ideal to operate within the nucleate boiling regime to capitalize on the high heat removal rate at low surface temperature. In addition, the ability to predict the critical heat flux (CHF), which denotes the departure from nucleate boiling regime, is also essential to prevent system burnout.

2.1.1 Nucleate boiling heat transfer

The classical boiling heat transfer model proposed by Rohsenow [15] and shown in Eq. (1) assumes that the heat removed from the surface is primarily due to the fluid motion induced by the departing bubbles or bubble microconvection. Hence, the single-phase force convection correlation was adopted where the bubble departure diameter and velocity were used as the characteristic length and velocity in the correlation. However, the effects of phase change were not considered.

$$q'' = \mu_l h_{fg} \left[\frac{g(\rho_l - \rho_g)}{\sigma}\right]^{\frac{1}{2}} \left[\frac{C_{pl}(T_w - T_{sat})}{C_{sf} h_{fg} \mathrm{Pr}_l^s}\right]^{\frac{1}{n}} \quad (1)$$

In a separate model, Mikic and Rohsenow [16] assumed that the departing bubble resulted in the removal of localized superheated liquid layer allowing cooler bulk fluid to replenish and cool the surface. Commonly known as the transient conduction model, this mechanism-based correlation shown in Eq. (2) includes the effects of the boiling surface active nucleation site density but does not consider interactions between neighboring bubbles.

$$\frac{q_t}{A_t} = \left(\frac{q}{A}\right)_b + \frac{A_{nc}}{A_t}\left(\frac{q}{A}\right)_{nc} \tag{2a}$$

$$\left(\frac{q}{A}\right)_b = \frac{K^2}{2}\sqrt{\pi k_l \rho_l C_{pl} f D_b^2 N (T_w - T_\infty)} \tag{2b}$$

For the laminar range, $10^5 < \mathrm{Ra} < 2 \times 10^7$,

$$\left(\frac{q}{A}\right)_{nc} = 0.54 \rho_l C_{pl} \left[\frac{\gamma g (T_w - T_\infty)^{\,5} \alpha^3}{\sqrt{A_{total}}\nu}\right]^{1/4} \tag{2c}$$

For the turbulent range, $2 \times 10^5 < \mathrm{Ra} < 3 \times 10^{10}$,

$$\left(\frac{q}{A}\right)_{nc} = 0.14 \rho_l C_{pl} \left[\frac{\gamma g (T_w - T_\infty)^{\,4} \alpha^2}{\nu}\right]^{1/3} \tag{2d}$$

Cooper and Lloyd [17] measured the surface temperatures of glass and ceramic substrates during the bubble ebullition cycle and recorded a rapid decline in temperature during the initial growth period of the vapor bubble. The temperature then quickly recovered following the formation of dry spot. This observation was consistent with the hypotheses of Snyder and Edward [18] and Moore and Mesler [19] and suggested that the dominant heat transfer mechanism during the ebullition cycle was the evaporation of the fluid microlayer beneath the growing bubble. To account for the effects of microlayer evaporation, Judd and Hwang [20] included an additional term shown in Eq. (3) to the right hand side of Eq. (2). Benjamin and Balakrishnan [21] subsequently derived an expression which relates the volume of the microlayer evaporation ($\bar{V}_{ME}$) to the bubble growth time.

$$\left(\frac{q}{A}\right)_{ME} = \rho_l h_{fg} N f \bar{V}_{ME} \tag{3}$$

On the other hand, Wayner et al. [22] showed that the significant heat transfer rate during the ebullition cycle was due to the evaporation of the thin liquid film at the three-phase contact line. Fig. 2 shows the liquid meniscus at the base of the bubble where the three-phase contact line exists. In the absorbed film region, the liquid film is of nanoscale thickness and cannot evaporate due to molecular adhesion force whereas in the micro region, maximum evaporation and heat transfer rates take place by heat conduction across the thin liquid film. Stephan and Hammer [23] included the effects of capillary pressure and interface curvature at the micro region and developed a model to predict the nucleate boiling heat transfer coefficient. From their numerical results, it was shown that the percentage of heat transfer from the micro region increases with increasing wall superheat and the maximum heat flux in the micro region was about 100 times larger than the burnout heat flux. Subsequently, Kern and Stephan [24] extended the model to binary fluid mixtures.

Building on the above earlier concepts, more comprehensive analytical and numerical boiling heat transfer models have subsequently been developed. For instance, Zhao et al. [25] suggested that the individual bubble growth can be divided into two distinct growth periods, viz., initial and final growth periods. In the initial growth period, the bubble grows from the evaporation of the microlayer whereas in the final growth period, the macrolayer (liquid layer thicker than the microlayer) forms underneath the bubble and between adjacent bubbles. Consequently, Das et al. [26] developed a mechanistic model which incorporated the mechanisms of near-wall micro-/macrolayer evaporation and transient conduction within the liquid layer. The model adopted several empirical constants but showed good agreement with experimental data obtained from the literature. More recently, a semi-analytical boiling heat transfer model was developed by Li et al. [27] for hydrophilic surfaces in which the influences of contact angle on the microlayer dynamics, bubble departure diameter and nucleation site density were considered. For hydrophilic surfaces with solid-liquid contact angles from 0° to 50°, the model showed reasonably good agreement with the experimental data (within ±30% error).

In order to investigate the nucleate boiling process, several numerical methods have also been introduced. Son et al. [28, 29] successfully implemented the level set (LS) method to simulate a single bubble growth process in which the LS formulation was coupled with the phase change equations to track the bubble liquid-vapor interface. On the other hand, Kunkelmann and Stephan [30] numerically studied the boiling of HFE-7100 using the Volume-of-Fluid (VOF) method. The effects of microscale heat transfer at the three-phase contact line was incorporated in the model and it was reported that the simulated bubble growth time and departure diameter were in good agreement with experimental observations. Recently, a modified VOF model was also developed by Jia et al. [31] through the introduction of an improved Height Function algorithm. Apart from the LS and VOF methods, the lattice Boltzmann method (LBM) provides another approach to solve the complex interfacial dynamics in the phase change process. LBM is a statistical mesoscopic method based on the kinetic theory where the system behavior is described by a distribution function. Gong and Cheng [32] proposed a LBM model for multiphase flow where the equation of state for real gas, which determined the system phase change, was incorporated in the body force term of the evolution equation. The ebullition cycle of a single bubble was simulated and results showed good agreement with existing correlations. The model was subsequently implemented to investigate boiling heat transfer on smooth surfaces with mixed wettability [33].

2.1.2 Bubble visualization

Microconvection, transient conduction, microlayer evaporation and three-phase contact line, as described above, are now recognized as the mechanisms associated with heat transfer in nucleate boiling although for many years, the extent to which each mechanism contributes to the ebullition heat transfer was not well established. However, since the early 2000s, significant progress in the fundamental understanding of the boiling phenomenon was achieved with the advancements in MEMS and imaging technologies. High precision and high resolution sensors, heaters and imaging devices were made available and were employed in numerous experimental studies with dielectric fluids. An important study was presented by Demiray and Kim [34] using an array of micro-sized heating elements (Fig. 3) to generate bubble nucleation from a single site. A feedback loop was set up to maintain the heaters at constant temperature and the investigations were conducted in FC-72 under subcooled conditions. Based on the instantaneous heat flux and high speed images recorded during the ebullition cycle of isolated bubbles, it was deduced that transient conduction and/or microconvection was the dominant

mechanism for bubble heat transfer. Subsequently, Myers et al. [35] extended the work to measurements of bubble nucleation under constant wall heat flux and determined that microlayer evaporation and contact line heat transfer account for not more than 23% of the total heat transfer from the surface. Wagner and Stephan [36], on the other hand, measured the evolution of a bubble from a single nucleation site using IR thermography. At 500 mbar, the ratio of the micro region heat flux ($q''_{mic,m}$) to the total bubble evaporation heat flux (q''_B) was 30% for FC-84 and was reduced to 13.2% for FC-84/FC-3284 binary mixtures. More recently, Moghaddam and Kiger [37, 38] investigated saturated boiling of FC-72 of a single bubble from an artificial cavity and obtained temperature measurements with spatial resolutions of 22 to 40 μm. From the temperatures recorded and the high speed images of the bubble evolution (Fig. 4), it was identified that the transient conduction mechanism was mainly limited to the bubble-to-surface contact area whereas microconvection was localized outside the contact area. In addition, heat transfer from microlayer evaporation only constituted between 16.3% and 28.8% of the total heat transfer.

Based on the published research highlighted above, it has been relatively well accepted that transient conduction and/or microconvection are the dominant mechanisms in the heat transfer of isolated bubbles. However, under high heat fluxes, significantly larger number of bubbles can be generated over the boiling surface which would result in interaction and coalescence of neighboring bubbles. Bubble interaction may alter the bubble dynamics such as bubble growth rate and departure frequency which may in turn affect the associated mode of heat transfer. Using a microheater array, Chen and Chung [39] generated two bubbles growing adjacent to each other and at close proximity such that the bubbles were allowed to touch and coalesce during the ebullition cycle. Their measurements indicated that bubble coalescence have increased the bubble departure frequency and also substantially enhanced heat transfer (up to 70%). On the other hand, from the observation of the high speed images taken (Fig. 5), Seidel et al. [40] reasoned that the occurrence of pressure imbalance at the instance of bubble coalescence created shock waves which propagated along two fronts. It was suggested that these capillary induced waves, instead of vapor production during bubble merger, resulted in the removal of the macrolayer beneath the coalesced bubbles. More recently, Bi et al. [41] studied the effects of coalescence of (1) two bubbles of identical sizes and (2) two bubbles of different sizes in FC-72. It was observed that the heat flux enhancement due to bubble coalescence was significantly larger than bubble growth and accounted for approximately 90% of the total increase in heat flux. Bubble coalescence also increased the bubble departure frequencies by more than two times as compared to single bubble growth and hence, resulted in the increase in average heat flux.

Apart from plain surfaces, the need for higher heat flux removal have also resulted in the introduction of numerous enhanced boiling surfaces such as surfaces with artificial fins, cavities and grooves. The various surface modification techniques and the associated heat transfer characteristics of these surfaces will be discussed in detail in Section 2.2. On the visualization of bubble dynamics, the presence of surface features have been shown to alter the bubble behavior and increased the complexity of transport mechanisms involved. For instance, artificial surface pores of various pore diameters (0.12 to 0.2 mm) with interconnected network channels were fabricated by Ramaswamy et al. [42]. In their bubble visualization studies in FC-72, for each surface of the same pore size and pore separation, data of approximately 50 bubbles were collected, from which the average bubble departure diameters (D_b) were computed. It was determined that D_b increases whereas the bubble departure frequency decreases with increasing pore diameter. In addition, the bubble growth rates were seen to increase linearly with time for the entire growth period, suggesting that the bubble growth was

inertia driven. Subsequent boiling visualization by Ghiu and Joshi [43] of similar enhanced surfaces made from transparent material (quartz) further determined that the evaporation process within the interconnected channels also contributed significantly to the overall heat dissipated from the surface. More recently, Teodori et al. [44] combined high speed visualization with Particle Imaging Velocimetry (PIV) and substrate surface temperature measurements to determine the effects of artificial cavity spacing on boiling. Enhanced surfaces with arrays of micro-sized square cavities (52 μm width and 20 μm depth) with different spacings were fabricated and tested in water, ethanol and HFE-7100. From their measurements, the bubble departure frequency was observed to increase with decreasing cavity spacing. In addition, for boiling from surfaces with closely spaced cavities in HFE-7000, stable increase in the heat transfer coefficient was observed with increasing bubble characteristics velocities. However, for surfaces with micro-cavities, horizontal coalescence of bubbles at high heat flux were suggested to have deteriorated heat transfer coefficients as the bubbles formed a vapor layer which insulated the surface and prevented liquid replenishments. Subsequent studies suggested that the horizontal bubble coalescence can be inhibited with the use of surface enhanced micro-sized pillars which delay the formation of the vapor blanket [45].

2.1.3 Critical heat flux

Despite coexisting on the continuous boiling curve as shown in Fig. 1, nucleate boiling heat transfer and CHF are conventionally viewed as disjoint processes dominated by different mechanisms. One of the earliest CHF model which was developed by Zuber [46] assumes that CHF occurs when the columns of vapor jets escaping from the boiling surface and the resupply fluid in the counterflow direction reached a hydrodynamically unstable state that inhibited further vapor outflow. Based on the Taylor and Helmholtz instabilities, Eq. (4) which relates CHF to the fluid thermophysical properties was derived where the constant, *C*, was taken to be 0.131. On the other hand, Gaertner [47] conducted visualization studies on the boiling phenomenon and reported the existence of a macrolayer, comprising columns of vapor stems and a liquid film between the heated surface and a hovering vapor mushroom at high heat flux. Assuming that the thickness of the macrolayer was related to Helmholtz instabilities at the interface of the vapor-liquid stems and that CHF occurs when the macrolayer dries out before the departure of the vapor mushroom, Haramura and Katto [48] developed a hydrodynamic model which relates CHF to the vapor stem-to-heater surface area ratio as shown in Eq. (5). The hydrodynamic models of Zuber [46] and Haramura and Katto [48] provide reasonably accurate predictions for a wide range of applications. Furthermore, Eq. (4) also allows the flexibility for *C* to be varied so as to correlate with the different boiling conditions. For instance, El-Genk and Parker [49] and Ho et al. [50] proposed *C* as a function of the surface orientation and correlated with the experimental CHF values of enhanced surfaces in dielectric fluids.

$$q''_{CHF} = C\rho_g^{1/2} h_{fg}\left[g\sigma\left(\rho_l - \rho_g\right)\right]^{1/4} \tag{4}$$

$$q''_{CHF} = 0.72\left(\frac{A_v}{A_w}\right)^{\frac{5}{8}}\left(1-\frac{A_v}{A_w}\right)^{\frac{5}{16}}\left[\frac{\left(\frac{\rho_l}{\rho_g}+1\right)}{\left(\frac{11}{16}\frac{\rho_l}{\rho_g}+1\right)^{3/5}}\right]^{\frac{5}{16}}\left\{\rho_g h_{fg}\left[\sigma g(\rho_l-\rho_g)\right]^{1/4}\right\} \tag{5}$$

However, the hydrodynamic models were also commonly criticized for not having explicit expressions to account for effects such as surface topology, surface wettability and material thermal conductivity. This led to several improved models being proposed in recent years. Arik

and Bar-Cohen [51] suggested that boiling surface properties such as heater thickness and thermal conductivity have direct influence on CHF and can be characterized using the thermal effusivity relation. Under high heat flux, surfaces of high effusivity facilitate the temperature rise at localized dry spots and caused heat to be conducted to regions of the surface where nucleate boiling still prevails. This prevents global dryout and delays CHF. The effusivity-based CHF correlation for dielectric fluids was developed, as shown in Eq. (6), and provided accurate predictions for a range of surfaces in dielectric fluids. On the other hand, the effects of surface-liquid interactions were considered in the CHF model proposed by Kandlikar [52] through the introduction of the contact angle (β) as shown in Eq. (7). The model suggests that CHF was caused by the uncontrolled lateral expansion of the bubble which eventually blanketed the heater surface and was derived by balancing the vapor recoil forces against the counteracting surface tension and gravitational forces acting on the bubble. The model was validated with fluids of different contact angles and surface orientations with reasonably accurate predictions.

$$q''_{CHF} = \frac{\pi}{24} h_{fg} \rho_g^{1/2} \left[\sigma g(\rho_l - \rho_g)\right]^{1/4} \left(\frac{S}{S+0.1}\right) \times \left[1 + \langle 0.3014 - 0.01507 L'(P) \rangle\right] \times \left(1 + 0.030 \left[\left(\frac{\rho_l}{\rho_g}\right)^{0.75} \frac{C_{pl}}{h_{fg}}\right] \Delta T_{sub}\right) \quad (6)$$

$$q''_{CHF} = h_{fg} \rho_g^{1/2} \left(\frac{1+\cos\beta}{16}\right) \left(\frac{2}{\pi} + \frac{\pi}{4}(1+cos\beta)\cos\phi\right)^{1/2} \left[\sigma(\rho_l - \rho_v)\right]^{1/4} \quad (7)$$

Certain micro/nanostructured enhanced surfaces exhibit very high surface wettability with apparent contact angles ranging from 0° to 20°. For these surfaces, substantial deviations between measured CHF values and predicted values from Eq. (7) were observed [53, 54]. Kim and Kim [53] characterized surface wettability using the capillarity of the surface. Increased surface capillarity facilitates the resupply of liquid to dry regions under high heat flux which further delays CHF. To account for the enhancement of CHF due to capillary wicking effects, Ahn et al. [54] modified Kandlikar's CHF model by including a scaling factor (A_1) to Eq. (7) and an additional term for capillarity effects, as shown in Eq. (8). On the other hand, Chu et al. [55] included Wenzel's equation [56] in their CHF model to account for the microscopic surface topology of silicon surfaces fabricated with arrays of micro-sized pillars. As shown in Eq. (9), CHF is related to the surface roughness factor (r), which can be calculated from the geometries of the surface micro-features, and the liquid receding angle on the corresponding smooth surface (θ_{rec}). Other models which account for the effects of microstructures topology have also been proposed by Zou and Maroo [57] and Rahman et al. [58]. More recently, Quan et al. [59] obtained a modified Taylor instability wavelength for microstructured surfaces by analyzing the change in surface free energy. Adopting the force balance approach of Kandlikar [52] and by including the effects of capillary wicking force and the modified Taylor wavelength, a CHF model as shown in Eq. (10) was developed. The model indicates the dependence of CHF on the microstructures surface features which are characterized by the surface roughness factor (r) and solid fraction (φ_s). The model was compared against existing experimental data for enhanced surfaces in water, ethanol and FC-72, and most of the predicted CHF values were found to be within ±25% of the experimental results.

$$q''_{CHF} = A_1 \times h_{fg}\rho_g^{1/2}\left(\frac{1+\cos\beta}{16}\right)\left(\frac{2}{\pi}+\frac{\pi}{4}(1+cos\beta)\cos\phi\right)^{1/2}[\sigma(\rho_l-\rho_v)\,]^{1/4} + \frac{\varepsilon\delta\rho_l h_{fg}A_2}{A_{heating}}\frac{dA_{wetted}}{dt} \quad (8)$$

$$q''_{CHF} = h_{fg}\rho_g^{1/2}\left(\frac{1+\cos\beta}{16}\right)\left(\frac{2(1+r\cos\theta_{rec})}{\pi(1+\cos\beta)}+\frac{\pi}{4}(1+cos\beta)\cos\phi\right)^{1/2}[\sigma(\rho_l - \rho_v)\,]^{1/4} \quad (9)$$

$$q''_{CHF} = h_{fg}\rho_g^{1/2}[\sigma(\rho_l-\rho_v)\,]^{1/4}\left(\frac{1+\cos\beta}{16}\right) \times\left(\frac{2}{\pi}(1-\sqrt{\varphi_s})\frac{r+\cos\beta}{1+\cos\beta}+\frac{\pi}{4}(1-\sqrt{\varphi_s})^{\frac{1}{2}}(1+cos\beta)\cos\phi\right)^{1/2} \quad (10)$$

2.2 Nucleate pool boiling of enhanced surfaces

Over the years, numerous enhanced surfaces were fabricated for improving nucleate boiling heat transfer in dielectric fluids. These surfaces can be broadly classified into (1) coated surfaces – surface features are directly coated onto the substrate surfaces, (2) intrinsic surfaces – surface features that are intrinsically part of the material's surface and (3) hybrid surfaces – surface features which consist of combinations of (1) and/or (2). In this section, the recent progress in nucleate pool boiling of dielectric fluids with enhanced surfaces is reviewed. An attempt is made to classify the surfaces based on their fabrication techniques. In addition, the various fabrication techniques employed are briefly summarized and the corresponding heat transfer performances of the enhanced surface are examined and compared.

2.2.1 Coated surfaces

Epoxy binding

One of the initial methods employed in the fabrication of enhanced surfaces is the direct coating of micro-sized particles onto plain surfaces using adhesive epoxies. Synthetic diamond particles were often used as the coating material due to its superior thermal conductivity. The coating forms porous structures with cavities which could increase the active nucleation site density [60]. Chang and You [61] investigated the pool boiling performances of surfaces coated with different sizes of diamond particles (2 μm to 70 μm) in saturated FC-72 and reported that the surface coated with 20 μm diamond particles exhibited the highest heat transfer coefficients under high heat fluxes (> 2.5 W/cm^2). Rainey and You [60] conducted comprehensive studies on the effects of surface orientation and heater size in saturated FC-72 and concluded that the coated surfaces were insensitive to these parameters. A subsequent analysis on the bubble dynamics by Kim et al. [62] on wire heaters showed that the diamond particle coating resulted in higher bubble departure frequencies and smaller bubble departure diameter as compared to an untreated surface. It was further suggested that the coated surfaces enhanced heat transfer through the increase in latent heat transfer at low heat fluxes and increased convection heat transfer at high heat fluxes. Arik et al. [63] showed that the effusivity-based CHF correlation [Eq. (6)] provided good predictions for diamond coated surfaces tested at various pressure and subcooling temperatures, with a deviation of ±15%.

Dipping and dripping processes

Takata et al. [64] demonstrated the use of dipping method in the coating of substrate surface with micro/nano-sized particles. The coating was achieved by polishing the copper substrate surface to mirror finish and subsequently cleaning the surface with hydrochloric acid and ethanol before dipping the substrate in TiO_2 suspension and heating the samples at 150ºC. Wu et al. [65], on the other hand, coated TiO_2 nanoparticles of 10 nm particle size using the dripping process. One drop of diluted TiO_2-ethanol solution was deposited and spread over the substrate surface. The substrate was then heated to 200ºC which evaporated the ethanol leaving 1 µm thickness of TiO_2 coating. TiO_2 was known for its high affinity for water and superhydrophilic surfaces with near 0º water-surface contact angle could be produced using TiO_2 coating. Enhanced boiling performances of TiO_2 coated surfaces in water were suggested to be due to the surface's increased water affinity [64]. However, even for highly wetting fluids such as FC-72, Wu et al. [65] demonstrated that significant boiling performances can be achieved with TiO_2 coating where improvements in heat transfer coefficients and CHF were up to 91.2% and 38.2% as compared to plain copper. The effective liquid-solid interactions induced by superhydrophilic TiO_2 coating was suggested for the enhancements observed.

Spray coating

In this method, coating is achieved by accelerating the coating particles at high velocities and impinging them directly onto the substrate surfaces. Due to the high impact experienced by the particles as they bombarded the surfaces, the particles undergo plastic deformation and adhere to the surfaces. In some instances, the coating precursors are also pre-heated or melted before spraying onto the surfaces. For instance, Dewangan et al. [66] coated copper powder onto horizontal copper tubes using a gas flame spraying technique and tested the surfaces in pure and quasi-azeotropic refrigerants. On the other hand, using the cold gas dynamic spraying method, Pialago et al. [67, 68] fabricated surfaces coated with carbon nanotubes (CNT)-metallic powder composites and performed their boiling experiments in R134a. Recently, Sahu et al. [69] coated polymer nanofibers onto the copper substrate by employing the electrically-assisted supersonic blowing technique. Air was blown out of a nozzle at supersonic velocity and 6 wt% PAN solution in DMF was pumped through a gage needle. An electric potential was set up between the needle and the nozzle to attract the polymer towards the nozzle which was then carried and impinged onto the substrate. To improve thermal conduction, electroplating was further carried out on the coated surfaces. These processes resulted in the formation of a copper-plated nanofiber mat as shown in Fig. 6. Employing a similar coating method, Sahu et al. [70] investigated the pool boiling heat transfer of copper-plated nanofiber coated surface and their results in HFE-7300 showed that CHF was 33% higher and significant enhancements in heat transfer coefficients were obtained as compared to an untreated copper surface. In addition, prolonged boiling has also resulted in a slight reduction in the nanofiber surface roughness although no change in the heat transfer characteristics of the surface was observed. Using supersonic spraying, a surface coated with reduced graphene oxide (rGO) was produced by An et al. [71] and their boiling experiments were performed in FC-72 at system pressure of 0.24 bar and fluid temperature of 20ºC. In comparison with a bare copper surface, the coating of rGO film improved heat transfer coefficients and CHF by 1.5 times and 0.5 times, respectively. The improved wettability and large number of boiling nucleation sites of the rGO film were suggested to have resulted in the improved heat transfer characteristics.

Free particles and particle sintering

The use of free particles in enhancing nucleate boiling heat transfer was demonstrated by Kim et al. [72]. In this method, the particles are free to move on the boiling surface. Copper particles were selected as the high density of copper makes the particles more resilient to removal from the surface by the departing bubbles during boiling. The narrow corner cavities formed by the free particles were suggested to have increased the number of surface nucleation sites. Various sizes of particles were investigated in FC-72 and an enhancement in the heat transfer coefficient of 76.3% and CHF of 160 kW/m^2 were achieved with the 10 μm particle size. Subsequently, the boiling performances of surfaces with sintered and free particles were studied by Sarangi et al. [73]. Free particles deposited surfaces similar to those reported by Kim et al. [72] were produced, while sintered coatings were fabricated by placement of copper substrates onto graphite molds packed with copper particles. The particles were then sintered at an elevated temperature of 950ºC (Fig. 7). Experiments in FC-72 showed that surfaces with sintered coating resulted in significantly higher heat transfer coefficients as compared to free particles and plain surfaces. For instance, the best performing sintered coating provided 95% reduction in wall superheat for particle sizes ranging from 90-106 μm. An investigation of sintered powder coated surfaces was also carried out by Thiagarajan et al. [74]. Copper-rich microparticles of 5-20 μm diameters were sintered onto copper substrates to produce different coating thicknesses. Experiments were conducted in HFE-7100 and enhancements in the heat transfer coefficient by 50-270% and CHF by 33-60% as compared to a plain surface were obtained. Based on bubble visualization performed and a heat flux partition model, it was suggested that the heat transfer enhancement was due to the significantly higher active nucleation site density on the sintered surfaces.

Electrochemical deposition

El-Genk and Ali [75, 76] and Ali and El-Genk [77, 78] employed the electrochemical process to fabricate copper microporous coated surfaces. In this fabrication technique, the copper substrate to be coated was positioned as the cathode in the electrolysis process, where an electrolyte solution of sulfuric acid and copper sulfate were used. A high current density (3 A/cm^2) was transmitted through the cathode and anode resulting in the deposition of copper nano-dendrites on the substrate. Due to the generation and departure of hydrogen bubbles during the chemical process, pores were formed and the coating thickness could be varied by controlling the duration of the process. Images illustrating the microporous structures obtained from the scanning electron microscope (SEM) are depicted in Fig. 8. El-Genk and Ali [75] performed saturated pool boiling experiments with porous surfaces of different coating thicknesses in PF-5060. For all the porous surfaces investigated, CHF was found to range from 22.7 W/cm^2 to 27.8 W/cm^2 with the surface superheats between 2.16 K to 12.89 K. The porous surface with the medium range coating thickness (171.1 μm) was recorded to have the highest CHF (27.8 W/cm^2) at the lowest wall superheat (2.16 K). Ali and El-Genk [77] subsequently studied the pool boiling heat transfer performance of microporous surfaces at different surface orientations. The experimental results revealed that for all surfaces, CHF and the corresponding wall superheats reduced with increasing surface inclinations. However the CHF for porous surfaces still outperformed plain copper surface at all surface orientations. For instance, at 180° surface inclination, the CHF values for 80 μm and 137 μm coating thicknesses were respectively 74% and 87% higher than the plain copper surface. Similarly, by using electrochemical deposition, Furberg and Palm [79] fabricated microporous structures and investigated their pool boiling heat transfer performance in both R134a and FC-72. Visualization of the bubble departure phenomenon using high speed imaging revealed that bubble coalescence took place between adjacent pores at medium to high heat fluxes (> 5

W/cm^2) whereas relatively low bubble coalescence was observed at low heat fluxes (2 W/cm^2). In addition, the bubble diameter from the porous surface was also found to be 10 to 30% smaller than plain surface whereas higher bubble departure frequency was detected. It was suggested that the enhanced heat transfer was due to evaporation of fluid within the porous structures and the interconnected porous network served as effective vapor escape paths.

Chemical vapor deposition

Chemical vapor deposition (CVD) enables highly ordered structures to be synthesized onto the substrate surface. A catalyst is usually deposited onto the surface and the synthesis process is typically performed by exposing the surface to volatile precursor and carrier gas. Several researchers have investigated the pool boiling performances of vertically aligned CNT coated surfaces produced by CVD technique. For instance, Ujereh et al. [80] fabricated multi-walled carbon nanotubes (MWCNT) arrays of different CNT densities and coating patterns. The MWCNTs are approximately 50 nm in diameter and 20 to 30 μm in height. Saturated pool boiling of FC-72 enhanced CHF by 45% and the fully-coated CNT surface also exhibited 450% enhancement in heat transfer coefficient as compared to bare silicon. Subsequently, Sathyamurthi et al. [81] studied the performance of MWCNT in saturated and subcooled pool boiling of PF-5060 dielectric fluid. CNT coatings of 9 and 25 μm thicknesses were synthesized on atomically smooth silicon substrates where moderate enhancements in heat transfer coefficients were observed as compared to bare silicon. More recently, Ho et al. [50] reported a detailed investigation on pool boiling of CNT-coated surface under different surface orientations in saturated FC-72. Using iron as catalyst and pure acetylene as the carbon source, highly aligned CNTs of 215 μm thickness were produced (Fig. 9). Enhancements in the average heat transfer coefficient and CHF of up to 86% and 42% were respectively achieved as compared to bare silicon. In addition, the increase in surface orientation was also shown to reduce the average heat transfer coefficient of the CNT-coated surface. Finally, a modified Rohsenow correlation was proposed to characterize the pool boiling curves of the surfaces at different orientations.

Selected publications on pool boiling with coated surfaces reviewed above are summarized in Table 2 and comparisons of the boiling curves of the better performing surfaces from the selected publications are reproduced in Fig. 10. The reported enhancements in the heat transfer coefficients of the coated surfaces vary from 32% to more than 17 times as compared to plain/reference surfaces whereas CHF increases between 10% and 87%. From this review, it can be seen that the numerous surface coating techniques presented have resulted in significantly enhanced boiling performance which made these techniques attractive for many cooling applications. However, as the coatings are not intrinsically part of the substrate surface, the associated thermal contact resistance between the coating and substrate and the tendency of the coating to degrade and peel over time are some of the disadvantages. However, these drawbacks could be overcome by intrinsic surface feature designs, where the microstructures are part of the material surface. In the following section, the techniques employed in the fabrication of intrinsic surfaces and their accompanying heat transfer performances shall be discussed.

2.2.2 Intrinsic surface features

Electrical discharge machining (EDM)

Electrical discharge machining (EDM) uses electrical discharges or sparks to remove material from a workpiece and thereby obtain the desired shapes and geometries. Guglielmini et al. [82] uses EDM to fabricate fin arrays of different configurations. Fin lengths of 3 mm or 6 mm and fin thicknesses of 0.4 mm or 1.0 mm were produced. Experiments were performed to examine the pool boiling characteristics of these surfaces in FC-72 under different saturation pressures. The maximum overall heat transfer coefficients were observed to increase with fin thickness and spacing but decrease with fin length. Similarly, Yu and Lu [83] also produced millimeter-size rectangular fin arrays of different fin dimensions and arrangements using EDM. Boiling experiments and visualizations were performed in saturated FC-72. The results indicated that closely-spaced and longer fins caused high flow resistance to the departing bubbles along the fin and delay departure of the bubbles at the base of the fin. In addition, the overall heat transfer coefficient also decayed rapidly as fin spacing decreased or fin length increased. A maximum CHF of 9.8×10^5 W/m^2 was achieved with 0.5 mm fin spacing and 4.0 mm fin length, which was 5 times higher than that for the plain surface.

Jones et al. [84] produced samples of different surface roughness using EDM. The samples were characterized using various surface roughness parameters and have average roughness (R_a) ranging from 1.08 μm to 10.0 μm. Experiments were conducted with FC-77 and water. The results indicated stronger influence of R_a on heat transfer coefficients with FC-77 as compared to water. The roughest surface achieved 210% higher heat transfer coefficients as compared to a polished surface in FC-77. High speed visualization experiments on the boiling phenomenon of polished and EDM-roughened surface were subsequently carried out by McHale and Garimella [85]. They reported that the EDM-roughened surface resulted in smaller bubble departure diameters and larger departure frequencies as compared to a polished surface for a given heat flux.

Mechanically roughened surfaces

The effects of surface roughness were also explored by El-Genk and Suszko [86] where the copper samples were prepared by ablating the surfaces with emery papers of different grit counts. Samples with R_a ranging from 0.039 μm to 1.79 μm were tested at different surface orientations in saturated PF-5060. For all the surfaces, the maximum heat transfer coefficients (h_{MNB}) for the downward-facing orientation were found to be approximately 40% of the upward-facing orientation. In addition, the h_{MNB} of 1.72 W/cm^2·K was also recorded for the rougher surface (R_a = 1.44 μm) whereas h_{MNB} of the polished surface was only 0.67 W/cm^2·K, which represents more than 150% enhancement due to the increased surface roughness. Visualization of the bubble dynamics on these surfaces by Suszko and El-Genk [87] showed that the smooth copper surface has higher bubble growth rate, departure diameter and detachment frequency than the rougher copper surfaces and, for all surfaces, the bubble growth rates were proportional to the square root of time indicating that the bubble growth was thermally driven. In addition, based on the results obtained, it was also concluded that the enhancement in heat transfer with increasing surfaces roughness was primarily due to the increase in surface active nucleation site density.

Micro/nano-electro-mechanical (MEMS/NEMS) processes

In the past two decades, MEMS/NEMS processes such as depositions, photolithography and etching that were commonly used in semiconductor device fabrication have also been explored to produce enhanced surfaces for promoting boiling. Highly-ordered micro/nano-size surface features could be produced with these processes. For example, arrays of microcavities with

mouth diameters of 50 µm to 200 µm have been fabricated by Yu et al. [88]. Honda et al. [89], on the other hand, produced micro-pin-fin arrays of 50 µm fin thickness and fin heights of 60 µm. Wei et al. [90], subsequently, extended the studies to include surfaces of five different pin fin geometries. Pool boiling results in FC-72 showed that the micro-pin-fin surfaces displayed distinctively steep boiling curves with very small change in wall superheat with increasing heat flux. Wei et al. [90] suggested that the steep boiling curve was due to the highly-structured and uniformly-distributed micro-pin-fins which resulted in the activation of the nucleation sites at almost the same wall superheat. More recently, micro-pin-finned surfaces were investigated by Xue et al. [91] under the effects of microgravity. In comparison with the boiling curves of the micro-pin-finned surfaces under normal gravity, microgravity showed insignificant effect on boiling heat transfer. Xue et al. [91] suggested that the independence of gravity was due to the micro-pin-fin structures which allowed sufficient supply of fluid to the heated surface by capillary driving force. Subsequently, a new model for predicting the bubble departure radius from the micro-pin-finned surface under microgravity was developed by Zhang et al. [92].

Open cell foams

Graphite and metallic foams are the two types of open cell foams that have been investigated for boiling heat transfer applications. Graphite foams can be produced from carbon-rich precursors (also known as pitch) where the final forms are obtained by processes such as blowing, carbonization and graphitization under inert and high temperature environment [93]. On the other hand, metallic foams can be fabricated using infiltration casting technique which is typically achieved by solidification of superheated liquid in high pressure and vacuum environment [94].

Experimental studies on pool boiling of metallic foams of different pore densities were conducted by several researchers [95, 96]. However, their investigations were performed in deionized water and surfactant solutions. On the other hand, detailed studies on the pool boiling performance of porous graphite foams in dielectric fluids have been reported by Leong et al. [97], Jin et al. [98], Pranoto et al. [99], El-Genk and Parker [100] and El-Genk [101]. As shown in Fig. 11 (a), graphite foams have spherical and interconnected pores which are favorable for bubble generation. In addition, the large surface-to-volume ratio and high bulk thermal conductivity (150 W/m·K) [93] also made graphite foams a promising material for enhanced boiling heat transfer applications. Leong et al. [97] investigated cubic graphite foams (“Pocofoam” and “Kfoam”) of different bulk thermal conductivities in FC-72. Their results indicated that the boiling thermal resistances (R_b) of graphite foams were approximately 2 times lower than a copper block even though they have lower bulk thermal conductivity. “Kfoam” exhibited slightly better boiling performance than “Pocofoam”. Jin et al. [98] studied the effects of graphite foams in FC-72 and HFE-7000 and determined that lower R_b was achieved with HFE-7000 when compared with FC-72. Pranoto et al. [99] subsequently extended the studies to include finned porous graphite as shown in Fig. 11 (b). The finned porous graphite, however, exhibited lower average heat transfer coefficients than the block graphite. Based on the high quality images of the boiling phenomenon, it was evident that larger bubble density was generated from the block graphite as compared to the finned graphite, suggesting that the internal pores of the graphite foam contributed significantly to the enhanced heat transfer performance. On the other hand, El-Genk and Parker [100] conducted detailed investigations on boiling performance of porous graphite in FC-72 and HFE-7100 under saturated and subcooled conditions and over a range of surface orientations. It was shown that up to 52.7% higher boiling heat transfer coefficient was achieved with porous graphite in FC-72 as compared to HFE-7100. In addition, the surface orientation had negligible effect on the

maximum heat transfer coefficient (h_B^*) of the porous graphite although h_B^* was seen to increase linearly with increasing subcooling.

Selective Laser melting (SLM)

Selective Laser Melting (SLM) is an additive manufacturing (AM) technique which utilizes a high-power laser source to melt and fuse the base metal powder layer-by-layer to form a three-dimensional geometry. This technique enables customized parts and highly complex designs to be fabricated based on the input from computer aided design (CAD) software. Due to these advantages, there has been an increasing use of SLM for producing functional heat transfer devices [102-104]. However, publications on enhancing nucleate boiling heat transfer by SLM are scarce. Ho et al. [105] explored the possibility of improving nucleate pool heat transfer of FC-72 by fabricating microstructured surfaces of different designs. Micro-cavity, micro-fin and micro-channel surfaces were produced from an aluminum alloy, AlSi10Mg, and their heat transfer performances were experimentally investigated in a water-cooled thermosyphon. The enhanced surfaces exhibit 63.5% increase in heat transfer coefficient as compared to a plain AlSi10Mg surface. In a separate investigation, Ho et al. [106] further evaluated the nucleate boiling characteristics of a plain AlSi10Mg surface fabricated by SLM against that of a commercially casted plain Al-6061 surface. The results indicated that the plain AlSi10Mg improved the heat transfer coefficient by 40.6% and CHF by 31% as compared to the plain Al-6061 surface. The enhanced thermal performance of the plain AlSi10Mg surface was attributed to the inherent microscale cavities and grooves that were formed as a result of the laser melting process. In addition, surfaces with arrays of micro-cavity and micro-fins of different configuration were also produced where further enhancements in the average heat transfer coefficient and CHF of 70% and 76% as compared to plain Al-6061 were recorded. While the graphite foams, as discussed above, consist of non-uniformly distributed pores of different pore sizes, the possibility of fabricating structured porous substrates for enhancing pool boiling using SLM was recently demonstrated by Wong and Leong [107]. The porous structures were engineered by replicating arrays of Octet-truss unit cells to form specimens of heights ranging from 2.5 mm to 10 mm as shown in Fig. 12. The structures were tested in saturated FC-72 and improvement in heat transfer coefficients and CHF of up to 91.7% and more than 100% were obtained respectively for the porous structures as compared to plain Al-6061.

Selected publications on pool boiling with intrinsic surfaces reviewed above are summarized in Table 3 and comparisons of the boiling curves of the better performing surfaces from selected publications are reproduced in Fig. 14.

2.2.3 Hybrid surfaces

The fabrication of hybrid surfaces usually involves two or more of the processes presented in Sections 2.2.1 and 2.2.2. For instance, McHale et al. [108] applied a particle sintering process followed by microwave-plasma CVD to produce enhanced surfaces with CNT arrays grown over sintered copper particles. The sintered copper particles were coated over the surface by the sintering process whereas CVD was employed to grow the CNTs. Their experiments in HFE-7300 showed that the hybrid surface resulted in the highest boiling heat transfer performance as compared to other enhanced surfaces. In addition, it is also interesting to note that the enhancement in CHF of the hybrid surface as compared to plain copper was also higher than the combined CHF enhancements of the enhanced surfaces produced by individual technique.

Im et al. [109], on the other hand, fabricated microgrooved surfaces deposited with flower-like copper oxide nanostructures. The microgrooves were created by cutting the surface using an automatic die saw whereas the flower-like nanostructures were deposited by immersing the surface into NaOH solution with $(NH_4)_2S_2O_8$ oxidant. Similar to McHale et al. [108], higher boiling heat transfer coefficient and CHF were achieved with the hybrid surface as compared to the enhanced surfaces fabricated by individual process. In addition, capillary wicking induced by the large surface-to-volume ratio was suggested as the primary mechanism for the enhancements observed.

Recently, hybrid surfaces were also developed by Patil and Kandlikar [110]. The surfaces consisted of micro-size open channels with microporous coating on the top of the channel fins. The open channels were fabricated by CNC machining whereas a two-stage electrodeposition technique was employed to achieve the preferential microporous coating. As explained by Patil and Kandlikar [110], and as illustrated in Fig. 13, this surface design allowed bubble nucleation to take place on the porous coating at the fin top whereas liquid circulation was generated in the microchannel. Hence, the additional nucleation sites on the porous coating and the current of fluid flow in the microchannels provided cohesive mechanisms for enhancing the pool boiling performance. Following Patil and Kandlikar [110], Jaikumar and Kandlikar [111] experimentally investigated similar hybrid surfaces with a fin top microporous coating but with varying microchannel sizes in FC-87 dielectric fluid. In all, the hybrid surface recorded 270% enhancement in CHF as compared to the plain surface and a maximum heat transfer coefficient of 20 $kW/m^2 \cdot K$ was achieved.

3. Flow boiling

3.1 Overview

Flow boiling occurs under the presence of a pump to introduce convective heat transfer and to allow orientation flexibility. Due to fluid convection, nucleate flow boiling heat transfer can exceed that of pool boiling. However, in comparison with pool boiling, the flow boiling process is additionally affected by factors such as fluid mass flux and vapor quality. In addition, the presence of a pump also creates additional system complexity and pressure drop is also an important consideration which affects the cost and size of the pumping system.

Boiling-dominated and convection-dominated modes are the two modes of heat transfer commonly observed in flow boiling processes. In the boiling-dominated mode, the heat transfer coefficient varies significantly as heat flux changes whereas in the convection-dominated mode, mass flux and vapor quality have more significant effects on the heat transfer coefficient.

Flow boiling can also be divided into different regimes, as shown in Fig. 15, namely bubbly flow, plug flow, slug flow, wavy flow and annular flow. Many researchers have presented correlations to predict flow boiling heat transfer performance and pressure drop [112-117]. Kandlikar [116] had compiled correlations for saturated two-phase flow boiling heat transfer inside horizontal and vertical tubes using a wide range of experimental data and 10 different fluids. Thome et al. [117] presented a comprehensive review of flow boiling heat transfer, two-phase pressure drops and flow patterns of ammonia and hydrocarbons applied in air-conditioning, refrigeration and heat pump systems.

3.2 Flow boiling in mini/microchannels

Flow boiling heat transfer can be enhanced in channels with small dimensions due to the increase of surface-to-volume ratio. The mini/microchannel can be fabricated by etching or mechanical cutting methods. Thome [118] presented a review of flow boiling mechanisms and models in mini and microchannels. A comprehensive review on the history, advances and challenges of flow boiling heat transfer in microchannel is covered by Kandlikar [119]. Bertsch et al. [120] compiled predictions from 25 heat transfer correlations using a wide range of experiments from 10 independent sources. The hydraulic diameter of the tubes and channels considered in all the experiments was 2 mm or smaller.

3.2.1 Flow boiling patterns in mini/microchannels

A microchannel is defined by Kandlikar and Grande [121] as a flow passage of hydraulic diameter between 10 and 200 μm with the consideration of manufacturing limits of small channels. However, the dimensions alone may not be a sufficient indication of the unique heat transfer mechanisms which occur in microchannels. The flow boiling patterns in microchannels are observed to deviate from macro-sized channels, which contribute to different heat transfer characteristics. Kew and Cornell [122] proposed bubble growth confinement within a channel as the parameter to differentiate between macroscale and microscale flow boiling. The confinement number (Co) was introduced as shown in Eq. (11). They set the threshold at Co = 0.5, where Co > 0.5 is for microscale and Co < 0.5 is for macroscale. Ong and Thome [123] extended the investigation and studied two-phase flow patterns using a photodiode laser signal system. They proposed a new dimensionless number to classify macroscale-to-microscale

transition. The Froude number (Fr) was used to account for the inertia and gravity forces. The liquid and vapor phase viscosity and density, Reynolds number (Re) and Weber number (We) were used to account for the viscous, surface tension and shear forces. The definitions of the Froude number, Reynolds number and Weber number are given in Eqs. (12), (13) and (14), respectively. The introduction of these dimensionless numbers helps to better account for the transition from surface tension-dominated isolated bubble flow to shear-dominated annular flow. More recently, Tibirica and Ribatski [124] have completed a review of the characterization of the transition between flow boiling under macroscale and microscale conditions.

$$\mathrm{Co} = \frac{1}{D}\sqrt{\frac{\sigma}{g(\rho_l-\rho_g)}} \tag{11}$$

$$\mathrm{Fr} = \frac{G^2}{\rho_l^2 g D} \tag{12}$$

$$\mathrm{Re} = \frac{GD}{\mu} \tag{13}$$

$$\mathrm{We} = \frac{G^2 D}{\sigma\rho} \tag{14}$$

Harirchian and Garimella [125] proposed a new transition criterion using the convective confinement number, which predicts the conditions under which microscale confinement effects are exhibited in flow boiling. The Boiling number (Bl), which is the nondimensional form of the heat flux, and Bond number (Bo), which is the ratio of buoyancy to surface tension forces, are introduced and shown in Eqs. (15) and (16). The convective confinement number is defined as the product of Reynolds number (Re) and the square root of Bo. It is shown that for flow boiling of FC-77, physical confinement in the microchannels exists for convective confinement numbers smaller than 160. Under this condition, thin film evaporation contributes to heat transfer in addition to nucleate boiling, and results in larger values of heat transfer coefficient compared to those cases in which no confinement is observed and nucleate boiling is dominant. A comprehensive flow regime is computed for FC-77 as shown in Fig 16.

$$\mathrm{Bl} = \frac{q''}{\mathrm{G}h_{fg}} \tag{15}$$

$$\mathrm{Bo} = \frac{g(\rho_l-\rho_g)D^2}{\sigma} \tag{16}$$

Kandlikar [126] used a scaling analysis to identify the relative effects of different forces on the flow boiling process at the microscale level. The different forces considered for scaling are inertia, surface tension, shear, gravity and evaporation momentum forces. Flow pattern transitions and stability for flow boiling of water and FC-77 were evaluated. It was found that surface tension and evaporation momentum forces are important at the microscale level. The elongated bubble/slug flow pattern is presented as a limiting factor in heat transfer of a microchannel, as shown in Fig. 17. This flow pattern is similar to the bubble growth and departure phases in pool boiling. Transient conduction/microconvection was proposed to be the dominant heat transfer mechanism associated with this flow pattern.

Wang et al. [127] experimentally studied flow boiling of FC-72 and ethanol in microchannels of high aspect ratios. The hydraulic diameters (d_h) of the microchannels considered were 571 μm, 762 μm and 1454 μm. Mass fluxes of 11.2 kg/m^2·s, 22.4 kg/m^2·s and 44.8 kg/m^2·s were investigated. High speed visualization was employed to capture the flow patterns. Periodic recoiling and re-wetting were captured for both liquids as shown in Fig 18.

3.2.2 Flow instabilities in mini/microchannel

Flow instabilities have been observed by researchers during flow boiling in microchannel. Hetsroni et al. [128] performed flow visualization on boiling in microchannel and observed explosive boiling with periodic wetting and dry-outs. Pressure drop oscillations were also observed and they tend to increase with increasing vapor quality. The study also showed the strong dependence of the heat transfer coefficient on the vapor quality. Wang et al. [129] performed flow boiling using water in microchannel and attributed the instability to periodic bubble expansion in both upstream and downstream directions, causing increase of wall temperature and pressure drop. Bogojevic et al. [130] further identified two types of flow instabilities, namely high amplitude/low frequency oscillations and low amplitude/high frequency oscillations. In order to reduce the effect of flow instabilities, Kosar et al. [131] introduced flow restrictors at the microchannel inlet. Kandlikar et al. [132] introduced artificial nucleation sites and pressure drop elements. The combination of fabricated nucleation sites in conjunction with the 4% area pressure drop elements completely eliminated the instabilities associated with the reverse flow although this was at the expense of higher pressure drop. In order to better understand the pressure drop issues, Kim and Mudawar [133] has compiled a comprehensive review on the prediction of two-phase frictional pressure drop for mini/microchannel saturated flow boiling. A wide range of working fluids, hydraulic diameters, mass fluxes and reduced pressures were considered.

3.2.3 *Size effects of mini/microchannels*

Harirchian and Garimella [134] investigated the effect of two-phase heat transfer coefficient and pressure drop on different sizes of microchannels. FC-77 was used as the coolant fluid. Seven different parallel microchannels with fixed depth 400 μm and widths between 100 and 5850 μm were fabricated using a dicing saw on a silicon chip. It was observed that the heat transfer coefficient was independent of microchannel width above 400 μm. For a microchannel of 100 μm width, occurrence of annular flow at a lower heat flux range resulted in high heat transfer coefficient, but the performance became similar to microchannels of other widths at high heat flux. The pressure drop of two-phase flow was observed to increase with decreasing microchannel width at a fixed heat flux. The optimum width was determined to be 400 μm for high transfer and pumping power. Harirchian and Garimella [135] further extended their work by performing experiments with five additional microchannel substrates with channel depths of 100 and 250 μm and widths ranging from 100 to 1000 μm. Flow visualizations and heat transfer results showed that the cross-sectional area of the microchannel is important instead of solely relying on width, depth or aspect ratio. It was observed that vapor confinement occurred readily in microchannel of cross-sectional area smaller than 0.089 mm^2. Under this threshold, contributions of nucleate boiling and liquid film evaporation were proposed to enhance heat transfer.

3.3 Flow boiling with enhanced surfaces

3.3.1 Intrinsic surfaces

Ma et al. [136] fabricated micro-pin-fins on chip surfaces by using a dry etching technique to enhance the boiling heat transfer of FC-72. Different fluid velocities, liquid subcooling and chip configuration were investigated in their study. It was found that all the micro-pin-finned surfaces showed considerable heat transfer enhancement and increased CHF compared to the smooth surface. They also stated that the CHF values for all surfaces increased with fluid velocity and subcooling. The heat transfer could also be increased by increasing fin height. Wei et al. [137] conducted flow boiling on a silicon chip with micro-pin-fins fabricated using dry etching technique. Sub-cooled flow boiling with different flow velocities of FC-72 were performed on the silicon chip. It shows that the boiling heat transfer can be enhanced by increasing the total surface area. The evaporation of superheated liquid within the confined gaps between fins and micro-convection caused by thermocapillary force due to the suction of a bubble hovering on the top of micro-pin-fins were proposed mechanisms which enhanced heat transfer. Guo et al. [138] further conducted sub-cooled flow boiling with impingement of FC-72 simultaneously on the micro-pin-finned silicon chip. They showed that the boiling heat transfer can be enhanced by increasing the total surface area and the jet impingement velocity. It was observed that a large jet impingement velocity caused more turbulence and micro-convection, which helped to improve heat transfer at high heat flux and to delay the occurrence of CHF. Krishnamurthy and Peles [139] conducted subcooled and saturated flow boiling experiments of HFE-7000 across a single row of inline micro pin fins entrenched in a microchannel. Heat transfer coefficient enhancement was observed for the microchannel with fins as compared to a plain microchannel. The enhancement was higher with increasing Reynolds number and it was attributed to the wake interaction between the pin fins and better fluid mixing.

3.3.2 Porous coated surfaces

Rainey et al. [140] studied flow boiling from microporous coated surfaces in sub-cooled FC-72. Their experimental results showed that microporous surfaces outperformed plain surfaces and enhanced the CHF. Ammerman and You [141] performed flow boiling using FC-87 on microporous coated surfaces. It was observed that the presence of coating resulted in boiling incipience at lower wall superheats, increased heat transfer coefficients and delay of CHF. The enhancement was attributed to the increased nucleation sites and bubble departure frequency. As compared to a plain surface, the coated surfaces were able to increase CHF between 14% and 36%. Sun et al. [142] coated copper particles of 20, 50 and 120 μm onto horizontal minichannels, with hydraulic diameters ranging from 0.49 mm to 1.26 mm. The coatings were produced by sintering spherical copper particles on the bottom surface of the channel. Heat transfer coefficients of between 7 and 10 times were achieved as compared to an uncoated surface. The confinement effect was also studied in their experiments. It was observed that the decrease in the channel size and liquid mass flux strengthened the confinement effect, resulting in the reduction in CHF values. Bai et al. [143] investigated flow boiling in parallel microchannels with metallic porous coatings. Anhydrous ethanol was used as the fluid and microchannels of hydraulic diameter of 540 μm were used. A solid-state sintering method was used to coat copper particles of 30, 55 and 95 μm in diameter. The surfaces with porous coatings experienced higher pressure drop as compared to the plain surface. This was attributed to the increased shear stress due to the higher surface roughness and induced turbulence caused by the porous coating. Heat transfer was enhanced by up to 90% for surfaces with porous coating particularly at low vapor quality regime although the enhancement diminished greatly when the vapor quality was greater than 0.25.

3.3.3 Porous foams

Porous foams with large surface-area-to-volume ratio, low density, and high bulk thermal conductivity can be used as boiling evaporators for high heat flux device systems. Fluid flow mixing is enhanced due to the increased tortuosity of porous foams. Kim et al. [144] performed flow boiling experiments of FC-72 in a foam-filled channel using copper foams of 10 and 20 pores per inch (PPI). It was reported that the increase of mass flux from 20 kg/m^2·s to 48 kg/m^2·s enhanced the heat transfer rate by as much as 15%. Further increase of the mass flux up to 72 kg/m^2·s did not enhance the cooling capability. The foam with a larger pore size was shown to have a better heat transfer characteristic as the vapor could escape more easily at high heat flux. Their experimental results showed that the high porosity and large pore size foam, i.e., the 95% and 10 PPI copper foam, gave the best result, achieving a heat transfer coefficient of 10 kW/m^2·K. Lu and Zhao [145] performed numerical and experimental analyses of flow boiling in horizontal metal foam tubes. It was found that the decrease in pore size with increase of pore density (PPI) resulted in significant improvement to the overall heat transfer performance due to the increase of surface area and strong flow mixing.

Graphite porous foams with high thermal conductivity were investigated by Pranoto and Leong [146] for flow boiling using FC-72. Two different graphite foams of 61% and 72% porosity were used. Evaporator gaps of 6, 4, and 2 mm were tested with coolant mass fluxes of 50, 100, and 150 kg/m^2·s. The experimental results show that the evaporator gap, coolant mass flux, and foam properties have effects on the flow boiling characteristics and performance. It was found that the use of foams of 61% and 72% porosity had enhanced the boiling heat transfer coefficients by up to 2.5 and 1.9 times, respectively as compared to those of a smooth surface. The better enhancement of the foam with 61% porosity is attributed to more active nucleation sites due to the higher surface-area-to-volume ratio. High speed visualization had confirmed the higher bubble departure frequency from the foam of 61% porosity.

Modeling of two-phase flow in porous foams is difficult due to the complexity of geometry and fluid-vapor motions. Li and Leong [147] numerically and experimentally investigated flow boiling of water and FC-72 in aluminum foams. The heat transfer process prior to the onset of nucleate boiling and the hysteresis effect were investigated. It was found experimentally that hysteresis occurred for water but was absent for FC-72. Numerical simulations were performed for both single- and two-phase heat transfer using the finite volume method. Reasonable agreements were obtained between the numerical and experimental results.

An experimental study of flow boiling heat transfer inside a channel filled with metallic foam was performed by Madani et al. [148]. A metallic copper foam of 36 PPI and 97% porosity and n-pentane were used in this study. The coolant mass flux and the heat flux were varied from 10 to 100 kg/m^2·s and 0 to 25 W/cm^2, respectively. Their experimental results showed that the heat transfer coefficient was enhanced by a factor from 2 to 4 as compared to the plain tube heat transfer coefficient calculated from the Gungor-Winterton correlation [149].

Selected publications on flow boiling with enhanced surfaces reviewed above are summarized in Table 4.

4. Concluding remarks

This paper critically reviews recent publications of pool and flow boiling of dielectric fluids over enhanced surfaces. The various models developed to characterize the nucleate boiling

curves and to predict critical heat fluxes of plain and enhanced surfaces and fundamental studies performed are analyzed and some of their benefits and shortcomings are highlighted. The numerous surface fabrication/modification techniques used in enhancing boiling heat transfer have achieved significant success over the last few decades. These fabrication/modification techniques are summarized in this paper and attempts are also made to categorize numerous enhanced surfaces reported in the literature. In addition, the heat transfer performances of these enhanced surfaces are also evaluated and their associated thermal transport mechanisms are elucidated.

Based on the above review conducted, the following areas which require further investigations are identified:

(1) While it has been shown through bubble visualization and temperature measurements that transient conduction and/or microconvection are the dominant mechanisms in heat transfer of isolated bubbles on plain surfaces [34-38], the effects of enhanced surface features on the bubble dynamics and the associated heat transfer mechanisms are still not well established. Parametric studies of enhanced surfaces such as micro-fin, micro-cavity or porous surfaces with different heights, diameters and pitches using high speed and high resolution visualization are therefore essential to achieve fundamental understanding of the bubble behavior and the mechanisms involved.

(2) In order to achieve fundamental understanding of the bubble behavior and the thermal transport mechanisms involved, appropriate surface modification/fabrication techniques have to be chosen. These modification/fabrication techniques should allow dimensions of the surface features (in the micro/nano-scale range) to be accurately manufactured. In this aspect, techniques such as MEMS/NEMS related processes and SLM have significant advantages over other techniques.

(3) The high nucleation site density of enhanced surfaces is a reason widely suggested for the observed improvements in boiling performance as compared to plain surfaces. However, the heat transfer coefficient and CHF are also strongly influenced by surface wettability. Despite the highly wetting nature of dielectric fluids, previous investigations suggest that significantly different heat transfer characteristics can also be achieved with enhanced surfaces of different wettabilities [65, 71]. There are, however, limited published studies in this area with dielectric fluids and more comparative studies are needed.

(4) Empirical and semi-empirical correlations for predicting the heat transfer and pressure drop performances of enhanced surfaces during boiling have achieved relative success. On the other hand, mechanism-based pool and flow boiling models for enhanced surfaces are limited. A fundamental understanding of the boiling mechanisms as mentioned in (1)-(3) is, therefore, essential for the development of accurate mechanism-based models.

(5) In order for the enhanced surfaces to be implemented in engineering systems, the reliability of the surfaces has to be evaluated. The surfaces should be subjected to systematic testing under extended durations so as to determine the change in boiling characteristics of these surfaces over time.

Acknowledgements

The authors would like to acknowledge the financial support under Nanyang Technological University Singapore's Academic Research Fund (AcRF) Tier 1 Grant No. RG 119/14 for recent studies on pool and flow boiling of surfaces fabricated by selective laser melting (SLM) reported in this review. Funding for the SLM facility by National Research Foundation, Singapore is gratefully acknowledged.

References

[1] Bar-Cohen, A., Holloway, C.A., Thermal science and engineering from macro to nano in 200 years, *Proceedings of the* 15th *International Heat Transfer Conference*, IHTC-15, August 10-15, Kyoto, Japan (2014).

[2] Mudawar, I., Assessment of high-heat-flux thermal management schemes, *IEEE Transactions on Components and Packaging Technologies*, Vol. 24, No. 2 (2001).

[3] Mudawar, I., Bharathan, D., Kelly, K., Narumanchi, S., Two-phase spray cooling of hybrid vehicle electronics, *Thermal and Thermomechanical Phenomena in Electronic Systems*, ITHERM, 11th Intersociety Conference, May 28-31, Orlando, USA (2008).

[4] Bar-Cohen, A., Thermal management of electronic components with dielectric liquid, *JSME International Journal Series B*, Vol. 36, no. 1, pp. 1-24 (1993).

[5] van Gils, R.W., Danilov, D., Notten, P.H.L., Speetjens, M.F.M., Nijmeijer, H., Battery thermal management by boiling heat-transfer, *Energy Conversion and Management*, Vol. 79, pp. 9-17 (2014).

[6] Bar-Cohen, A., Arik, M., Ohadi, M., Direct liquid cooling of high flux micro and nano electronic components, *Proceedings of the IEEE*, Vol. 94, No. 8, pp. 1549-1570 (2006).

[7] Kakaç S., Yurucu H., Hijikata K.A., *Cooling of Electronic Systems*, Kluwer Academic Publishers (1994).

[8] Ciloglu, D., Bolukbasi, A., A comprehensive review on pool boiling of nanofluids, *Applied Thermal Engineering*, Vol. 84, pp. 45-63 (2015).

[9] Fang, X., Wang, R., Chen, W., Zhang, H., Ma, C., A review of flow boiling heat transfer of nanofluids, *Applied Thermal Engineering*, Vol. 91, pp. 1003-1017 (2015).

[10] Patil, C.M., Kandlikar, S.G., Review of the manufacturing techniques for porous surfaces used in enhanced pool boiling, *Heat Transfer Engineering*, Vol. 35, pp. 887-902 (2014).

[11] Shojaeian, M., Kosar, A., Pool boiling and flow boiling on micro- and nanostructured surfaces, *Experimental Thermal and Fluid Science*, Vol. 63, pp. 45-73 (2015).

[12] Kim, D.E., Yu, D.I., Jerng, D.W., Kim, M.H., Ahn, H.S., Review of boiling heat transfer enhancement on micro/nanostructured surfaces, *Experimental Thermal and Fluid Science*, Vol. 66, pp. 173-196 (2015).

[13] 3M^{TM} Fluorinert^{TM} Electronic and Novec^{TM} Engineering Liquids product information, www.3m.com/fluids, 3M Corporation.

[14] Nukiyama, S., The maximum and minimum values of the heat Q transmitted from metal to boiling water under atmospheric pressure, *International Journal of Heat and Mass Transfer*, Vol. 9, pp. 1419-1433 (1966).

[15] Rohsenow, W.M., A method of correlating heat transfer data for surface boiling of liquids, *Transactions of ASME*, Vol. 74, pp. 969-967 (1952).

[16] Mikic, B.B., Rohsenow, M.W., A new correlation of pool-boiling data including the effect of heating surface characteristics, *Journal of Heat Transfer*, Vol. 9, pp. 245-250 (1969).

[17] Cooper, M.G., Lloyd, A.J.P, The microlayer in nucleate boiling, *International Journal of Heat and Mass Transfer*, Vol. 12, pp. 895-913 (1969).

[18] Snyder, N.R., Edwards, D.K., *Summary of conference on bubble dynamics and boiling heat transfer*, Jet Propulsion Laboratory Memo, 20, pp. 20-137 (1956).

[19] Moore, F.D., Mesler, R.B., The measurement of rapid surface temperature fluctuations during nucleate boiling of water, *AIChE*, Vol. 7, pp. 620-624 (1961).

[20] Judd, R.L., Hwang, K.S., A comprehensive model for nucleate boiling heat transfer, including microlayer evaporation, *Journal of Heat Transfer*, Vol. 98, pp. 623-629 (1976).

[21] Benjamin, R.J., Balakrishnan, A.R., Nucleate pool boiling heat transfer of pure liquids at low to moderate heat fluxes, *International Journal of Heat and Mass Transfer*, Vol. 39, pp. 2495-2504 (1996).

[22] Wayner, P.C., Kao, Y.K., LaCroix, L.V., The interline heat-transfer coefficient of an evaporating wetting film, *International Journal of Heat and Mass Transfer*, Vol. 19, pp. 487-492 (1976).

[23] Stephan, P., Hammer, J., A new model for nucleate boiling heat transfer, *Wärme- and Stoffübertragung*, Vol. 30, pp. 119-125 (1994).

[24] Kern, J., Stephan, P., Theoretical model for nucleate boiling heat and mass transfer of binary mixtures, *Journal of Heat Transfer*, Vol. 125, pp. 1106-1115 (2003).
[25] Zhao, Y.-H., Masuoka, T., Tsuruta, T., Unified theoretical prediction of fully developed nucleate boiling and critical heat flux based on a dynamic microlayer model, *International Journal of Heat and Mass Transfer*, Vol. 45, pp. 3189-3197 (2002).
[26] Das, A.K., Das, P.K., Saha, P., Heat transfer during pool boiling based on evaporation from micro and macrolayer, *International Journal of Heat and Mass Transfer*, Vol. 49, pp. 3487-3499 (2006).
[27] Li Y.-Y., Liu, Z.-H., Wang, G.-S., A predictive model of nucleate pool boiling on heated hydrophilic surfaces, *International Journal of Heat and Mass Transfer*, Vol. 65, pp. 789-797 (2013).
[28] Son, G., Dhir, V.K., Ramanujapu, N., Dynamics and heat transfer associated with a single bubble during nucleate boiling on a horizontal surface, *Journal of Heat Transfer*, Vol. 121, pp. 623-631 (1999).
[29] Son, G., Ramanujapu, N., Dhir, V.K., Numerical simulation of bubble merger process on a single nucleation site during pool nucleate boiling, *Journal of Heat Transfer*, Vol. 124, pp. 51-62 (2002).
[30] Kunkelmann, C., Stephan, P., Numerical simulation of the transient heat transfer during nucleate boiling of refrigerant HFE-7100, *International Journal of Refrigeration*, Vol. 33, pp.1221-1228 (2010).
[31] Jia, H.W., Zhang, P., Fu, X., Jiang, S.C., A numerical investigation of nucleate boiling at a constant surface temperature, *Applied Thermal Engineering*, Vol. 88, pp. 248-257 (2015).
[32] Gong, S., Cheng, P., Lattice Boltzmann simulation of periodic bubble nucleation, growth and departure from a heated surface in pool boiling, *International Journal of Heat and Mass Transfer*, Vol. 64, pp. 122-132 (2013).
[33] Gong, S., Cheng, P., Numerical simulation of pool boiling heat transfer on smooth surfaces with mixed wettability by lattice Boltzmann method, *International Journal of Heat and Mass Transfer*, Vol. 80, pp. 206-216 (2015).
[34] Demiray, F., Kim, J., Microscale heat transfer measurements during pool boiling of FC-72: effect of subcooling, *International Journal of Heat and Mass Transfer*, Vol. 47, pp. 3257-3268 (2004).
[35] Myers, J.G., Yerramilli, V.K., Hussey, S.W., Yee, G.F., Kim, J., Time and space resolved wall temperature and heat flux measurements during nucleate boiling with constant heat flux boundary conditions, *International Journal of Heat and Mass Transfer*, Vol. 48, pp. 2429-2442 (2005).
[36] Wagner, E., Stephan, P., High-resolution measurements at nucleate boiling of pure FC-84 and FC-3284 and its binary mixtures, *Journal of Heat Transfer*, Vol. 131, pp. 121008-1 - 121008-12 (2009).
[37] Moghaddam, S., Kiger, K., Physical mechanisms of heat transfer during single bubble nucleate boiling of FC-72 under saturation conditions-I. Experiment investigation, *International Journal of Heat and Mass Transfer*, Vol. 52, pp. 1284-1294 (2009).
[38] Moghaddam, S., Kiger, K., Physical mechanisms of heat transfer during single bubble nucleate boiling of FC-72 under saturation conditions-II. Theoretical analysis, *International Journal of Heat and Mass Transfer*, Vol. 52, pp. 1295-1303 (2009).
[39] Chen, T., Chung, J.N., Coalescence of bubbles in nucleate boiling on microheaters, *International Journal of Heat and Mass Transfer*, Vol. 45, pp. 2329-2341 (2002).
[40] Seidel, S., Cioulachtjian, S., Bonjour, J., Experimental analysis of bubble growth, departure and interactions during pool boiling on artificial nucleation sites, *Experimental Thermal and Fluid Science*, Vol. 32, pp. 1504-1511 (2008).
[41] Bi, J., Lin, X., Chistopher, D.M., Effects of bubble coalescence dynamics on heat flux distributions under bubbles, *AIChE*, Vol. 59, pp. 1735-1745 (2013).
[42] Ramaswamy, C., Joshi, Y., Nakayama, W., Johnson, W.B., High-speed visualization of boiling from an enhanced surface, *International Journal of Heat and Mass Transfer*, Vol. 45, pp. 4761-4771 (2002).
[43] Ghiu, C-D., Joshi, Y.K., Visualization study of pool boiling from thin confined enhanced structures, *International Journal of Heat and Mass Transfer*, Vol. 45, pp. 4287-4299 (2005).
[44] Teodori, E., Moita, A.S., Moreira, A.L.N., Study of the combined effects of liquid properties and surface micropatterning on pool boiling heat transfer, *Proceedings of the* 15th *International Heat Transfer Conference*, IHTC-15, August 10-15, Kyoto, Japan (2014).

[45] Moita, A.S., Teodori, E., Moreria, A.L.N., Influence of surface topography in the boiling mechanisms, *International Journal of Heat and Fluid Flow*, Vol. 52, pp. 50-63 (2015).
[46] Zuber, N., *Hydrodynamic Aspects of Boiling Heat Transfer*, AEC Report No. AECU-4439 (1959).
[47] Gaertner, R.F., Photographic study of nucleate pool boiling on a horizontal surface, *Journal of Heat Transfer*, Vol. 87, pp. 17-29 (1965).
[48] Haramura,Y., Katto, Y., A new hydrodynamic model of critical heat flux applicable widely to both pool and forced convection boiling on submerged bodies in saturated liquids, *International Journal of Heat and Mass Transfer*, Vol. 3, pp. 389-399 (1983).
[49] El-Genk, M., Parker, J.L., Nucleate boiling of FC-72 and HFE-7100 on porous graphite at different orientations and liquid subcooling, *Energy Conversion and Management*, Vol. 49, pp. 733-750 (2008).
[50] Ho, J.Y., Leong, K.C., Yang, C., Saturated pool boiling from carbon nanotube surfaces at different orientations, *International Journal of Heat and Mass Transfer*, Vol. 79, pp. 893-904 (2014).
[51] Arik, M., Bar-Cohen, A., Effusivity-based correlation of surface property effects in pool boiling CHF of dielectric liquids, *International Journal of Heat and Mass Transfer*, Vol. 46, pp. 3755-3764 (2003).
[52] Kandlikar, S.G., A theoretical model to predict pool boiling CHF incorporating effects of contact angle and orientation, *Journal of Heat Transfer*, Vol. 123, pp. 1071-1079 (2001).
[53] Kim, H.D., Kim, M.H., Effect of nanoparticle deposition on capillary wicking that influences the critical heat flux in nanofluids, *Applied Physics Letters*, Vol. 91, pp. 014104 (2007).
[54] Ahn, H.S, Lee, C., Kim, J., Kim, M.H., The effect of capillary wicking action of micro/ nano structures on pool boiling critical heat flux, *International Journal of Heat and Mass Transfer*, Vol. 55, pp. 89-92 (2012).
[55] Chu, K-H., Enright, R., Wang, E.N., Structured surfaces for enhanced pool boiling heat transfer, *Applied Physics Letters*, Vol. 100, pp. 241603 (2012).
[56] Wenzel, R.N., Resistance of solid surface to wetting by water, *Industrial and Engineering Chemistry*, Vol. 28, pp. 988-994 (1936).
[57] Zou, A., Maroo, S.C., Critical height of micro/nano structures for pool boiling heat transfer enhancement, *Applied Physics Letters*, Vol. 103, pp. 221602 (2013).
[58] Rahman, M.M., Ölçeroğlu,, E., McCarthy, M., Role of wickability on the critical heat flux of structured superhydrophilic surface, *Langmuir*, Vol. 30, pp. 11225-11234 (2014).
[59] Quan, X., Dong, L., Cheng, P., A CHF model for saturated pool boiling on a heated surface with micro/nano-scale structures, *International Journal of Heat and Mass Transfer*, Vol. 76, pp. 452-458 (2014).
[60] Rainey, K.N., You, S.M., Effect of heater size and orientation on pool boiling heat transfer from microporous coated surfaces, *International Journal of Heat and Mass Transfer*, Vol. 44, pp. 2589-2599 (2001).
[61] Chang, J.Y., You, S.M., Boiling heat transfer phenomena from micro-porous and porous surfaces in saturated FC-72, *International Journal of Heat and Mass Transfer*, Vol. 40, pp. 4437-4447 (1997).
[62] Kim, J.H., Rainey, K.N., You, S.M., Pak, J.Y., Mechanism of nucleate boiling heat transfer enhancement from microscopic surfaces in saturated FC-72, *Journal of Heat Transfer*, Vol. 124, pp. 500-506 (2002).
[63] Arik, M., Bar-Cohen, A., You, S.M., Enhancement of pool boiling critical heat flux in dielectric liqiuds by microscopic coatings, *International Journal of Heat and Mass Transfer*, Vol. 50, pp. 997-1009 (2007).
[64] Takata, Y., Hidaka, S., Cao, J.M., Nakamura, T., Yamamoto, H., Masuda, M., Ito, T., Effect of surface wettability on boiling and evaporation, *Energy*, Vol. 30, pp. 209-220 (2005).
[65] Wu, W., Bostanci, H., Chow, L.C., Hong, Y., Su, M., Kizito, J.P., Nucleate boiling heat transfer enhancement for water and FC-72 on titanium oxide and silicon oxide surfaces, *International Journal of Heat and Mass Transfer*, Vol. 53, pp. 1773-1777 (2010).
[66] Dewangan, A.K., Kumar, A., Kumar, R., Nucleate boiling of pure and quasi-azeotropic refrigerants from copper coated surfaces, *Applied Thermal Engineering*, Vol. 94, pp. 395-403 (2016).
[67] Pialago, E.J.T., Kwon, O.K., Park, C.W., Nucleate boiling heat transfer of R134a on cold sprayed CNT-Cu composite coatings, *Applied Thermal Engineering*, Vol. 56, pp. 112-119 (2013).

[68] Pialago, E.J.T., Kwon, O.K., Jin, J.S., Park, C.W., Nucleate pool boiling of R134a on cold sprayed Cu-CNT-SiC and Cu-CNT-AIN composite coatings, *Applied Thermal Engineering*, Vol. 103, pp. 648-694 (2016).
[69] Sahu, R.P., Sinha-Ray, S., Sinha-Ray, S., Yarin, A.L., Pool boiling on nano-tectured surfaces comprised of electrically-assisted supersonically soluation-blown, copper-plated nanofibers: Experiments and theory, *International Journal of Heat and Mass Transfer*, Vol. 87, pp. 521-535 (2015).
[70] Sahu, R.P., Sinha-Ray, S., Sinha-Ray, S., Yarin, A.L., Pool boiling of Novec 7300 and self-rewetting fluids on electrically-assisted supersonically soluation-blown, copper-plated nanofibers, *Intenrational Journal of Heat and Mass Transfer*, Vol. 95, pp. 83-93 (2016).
[71] An, S., Kim, D-Y., Lee, J-G., Jo, H.S., Kim, M.W., Al-Deyab, S.S., Choi, J., Yoon S.S., Supersonically sprayed reduced graphene oxide film to enhance critical heat flux in pool boiling, *International Journal of Heat and Mass Transfer*, Vol. 98, pp. 124-130 (2016).
[72] Kim, T.Y., Weibel, J.A., Garimella, S.V., A free-particles-based technique for boiling heat transfer enhancement in a wetting liquid, *International Journal of Heat and Mass Transfer*,Vol. 71, pp. 808-817 (2014).
[73] Sarangi, S., Weibel, J.A., Garimella, S.V., Effect of particle size on surface-coating enhancement of pool boiling heat transfer, *International Journal of Heat and Mass Transfer*, Vol. 81, pp. 103-113 (2015).
[74] Thiagarajan, S.J., Yang, R., King, C., Narumanchi, S., Bubble dynamics and nucleate pool boiling heat transfer on microporous copper surfaces, *International Journal of Heat and Mass Transfer*, Vol. 89, pp. 1297-1315 (2015).
[75] El-Genk, M.S., Ali, A.F., Enhanced nucleate boiling on copper micro-porous surfaces, *International Journal of Multiphase Flow*, Vol. 36, pp. 780-792 (2010).
[76] El-Genk, M.S., Ali, A.F., Enhancement of saturation boiling of PF-5060 on microporous copper dendrite surfaces, *Journal of Heat Transfer*, Vol. 132, pp. 071501-1 - 071501-9 (2010).
[77] Ali, A.F., El-Genk, M.S., Spreaders of immersion nucleate boiling cooling of a computer chip with a central hot spot, *Energy Conversion and Management*, Vol. 53, pp. 259-267 (2012).
[78] Ali, A.F., El-Genk, M.S., Effect of inclination on saturation boiling of PF-5060 dielectric liquid on 80- and 137-μ thick copper micro-porous surfaces, *International Jouranl of Thermal Sciences*, Vol. 53, pp. 42-48 (2012).
[79] Furberg, R., Palm, B., Boiling heat transfer on a dendritic and micro-porous surface in R134a and FC-72, *Applied Thermal Engineering*, Vol. 31, pp. 3595-3603 (2011).
[80] Ujereh, S., Fisher, T., Mudawar, I., Effects of carbon nanotubes arrays on nucleate pool boiling, *International Journal of Heat and Mass Transfer*, Vol. 50, pp. 4023-4038 (2007).
[81] Sathyamurthi, V., Ahn, H-S., Banerjee, D., Lau, S.C., Subcooled pool boiling experiments on horizontal heaters coated with carbon nanotubes, *Journal of Heat Transfer*, Vol. 131, pp. 071501-1 - 071501-10 (2009).
[82] Guglielmini, G., Misale, M., Schenone, C., Boiling of saturated FC-72 on square pin fin arrays, *International Journal of Thermal Sciences*, Vol. 41, pp. 599-608 (2002).
[83] Yu, C.K., Lu, D.C., Pool boiling heat transfer on horizontal rectangular fin array in saturated FC-72, *International Journal of Heat and Mass Transfer*, Vol. 50, pp. 3624-3637 (2007).
[84] Jones, B.J., McHale, J.P., Garimella, S.V., The influence of surface roughness on nucleate pool boiling heat transfer, *Journal of Heat Transfer*, Vol 131, pp. 121009-1 - 121009-14 (2009).
[85] McHale, J.P., Garimella, S.V., Bubble nucleation characterisitics in pool boiling of a wetting liquid on smooth and rough surfaces, *International Journal of Multiphase Flow*, Vol 36, pp. 249-260 (2009).
[86] El-Genk, M.S., Suszko, A., Saturated nucleate boiling and correlations for PF-5060 dielectric liquid on inclined rough copper surfaces, *Journal of Heat Transfer*, Vol 136, pp. 081503-1 - 081503-10 (2014).
[87] Suszko, A., El-Genk, M.S., Saturation boiling of PF-5060 on rough Cu surfaces: Bubbles transient growth, departure diameter and detachment frequency, *International Journal of Heat and Mass Transfer*, Vol 91, pp. 363-373 (2015).

[88] Yu, C.K., Lu, D.C., Cheng, T.C., Pool boiling heat transfer on artificial micro-cavity surfaces in dielectric fluid FC-72, *Journal of Micromechanics and Microengineering*, Vol. 16, pp. 2092-2099 (2006).
[89] Honda, H., Takamatsu, H., Wei, J.J., Enhanced boiling of FC-72 on silicon chips with micro-pin-fins and submicron-scale roughness, *Journal of Heat Transfer*, Vol. 124, pp. 383-390 (2002).
[90] Wei, J.J., Guo, L.J., Honda, H., Experimental study of boiling phenomena and heat transfer performances of FC-72 over micro-pin-finned silicon chips, *Heat and Mass Transfer*, Vol. 41, pp. 744-755 (2005).
[91] Xue, Y-F., Zhao, J-F., Wei, J-J., Zhang, Y-H., Qi, B-J., Experimental study of nucleate pool boiling of FC-72 on micro-pin-finned surface under microgravity, *International Journal of Heat and Mass Transfer*, Vol. 63, pp. 425-433 (2013).
[92] Zhang, Y., Wei, J., Xue, Y., Kong, X., Zhao, J., Bubble dynamics in nucleate pool boiling on micro-pin-finned surfaces in microgravity, *Applied Thermal Engineering*, Vol. 70, pp. 172-182 (2014).
[93] Gallego, N.C., Klett, J.W., Carbon foams for thermal management, *Carbon*, Vol. 41, pp. 1461-1466 (2003).
[94] Leong, K.C., Jin, L.W., Effect of oscillatory frequency on heat transfer in metal foam heat sinks of various pore densities, *International Journal of Heat and Mass Transfer*, Vol. 49, pp. 671-681 (2006).
[95] Xu, Z.G., Zhao, C.Y., Experimental study on pool boiling heat transfer in gradient metal foams, *International Journal of Heat and Mass Transfer*, Vol. 85, pp. 824-829 (2015).
[96] Xu, Z.G., Zhao, C.Y., Enhanced boiling heat transfer by gradient porous metals in saturated pure water and surfactant solutions, *Applied Thermal Engineering*, Vol. 100, pp. 68-77 (2016).
[97] Leong, K.C., Jin, L.W., Pranoto, I., Li, H.Y., Chai, J.C., Experimental study of enhanced pool boiling heat transfer using graphite foam inserts, *Defect and Diffusion Forum*, Vol. 312-315, pp. 352-357 (2011).
[98] Jin, L.W., Leong, K.C., Pranoto, I., Saturated pool boiling heat transfer from highly conductive graphite foams, *Applied Thermal Engineering*, Vol. 31, pp. 2685-2693 (2011).
[99] Pranoto, I., Leong, K.C., Jin, L.W., The role of graphite foam pore structure on saturated pool boiling enhancement, *Applied Thermal Engineering*, Vol. 42, pp. 163-172 (2012).
[100] El-Genk, M.S., Parker, J.L., Enhanced boiling of HFE-7100 dielectric liquid on porous graphite, *Energy Conversion and Management*, Vol. 46, pp. 2455-2481 (2005).
[101] El-Genk, M.S., Immersion cooling nucleate boiling of high power computer chips, *Energy Conversion and Management*, Vol. 53, pp. 205-218 (2012).
[102] Wong, M., Owen, I., Sutcliffe, C.J., Puri, A., Convective heat transfer and pressure losses across novel heat sinks fabricated by selective laser melting, *International Journal of Heat and Mass Transfer*, Vol. 52, pp. 281-288 (2009).
[103] Ventola, L., Robotti, F., Dialameh, M., Calignano, F., Manfredi, D., Chiavazo, E., Asinari, P., Rough surfaces with enhanced heat transfer of electronic cooling by direct laser sintering, *International Journal of Heat and Mass Transfer*, Vol. 75, pp. 58-74 (2014).
[104] Ameli, M., Agnew, B., Leung, P.S., Ng, B., Sutcliffe, C.J., Singh, J., McGlen, R., A novel method for manufacturing sintered aluminum heat pipes (SAHP*), Applied Thermal Engineering*, Vol. 52, pp. 498-504 (2013).
[105] Ho, J.Y., Wong, K.K., Leong, K.C., Yang, C., Enhanced nucleate pool boiling from microstructured surfaces fabricated by selective laser melting, *ASME* 2016 5th *Micro/Nanoscale Heat and Mass Transfer International Conference*, MNHMT-2016, January 3-6, Biopolis, Singapore (2016).
[106] Ho, J.Y., Wong, K.K., Leong, K.C., Saturated pool boiling of FC-72 from enhanced surfaces produced by selective laser melting, *International Journal of Heat and Mass Transfer*, Vol. 99, pp. 107-121 (2016).
[107] Wong, K.K., Leong, K.C., Pool boiling enhancement of porous structures fabricated by selective laser melting, *Proceedings of the International Symposium of Heat Transfer and Heat Powered Cycles*, IHTS-2016, 27-29 June, Nottingham, United Kingdom (2016).

[108] McHale, J.P., Garimella, S.V., Fisher, T.S., Powell, G.A., Pool boiling performance comparison of smooth and sintered copper surfaces with and without carbon nanotubes, *Nanoscale and Microscale Thermophysical Engineering*, Vol. 15, pp. 133-150 (2011).
[109] Im, Y., Dietz, C., Lee, S.S., Joshi, Y., Flower-like CuO nanostructures for enhanced boiling, *Nanoscale and Microscale Thermophysical Engineering*, Vol. 16, pp. 145-153 (2012).
[110] Patil, C.M., Kandlikar, S.G, Pool boiling enhancement through microporous coatings selectively electrodeposited on fin tops of open microchannels, *International Journal of Heat and Mass Transfer*, Vol. 79, pp. 816-828 (2014).
[111] Jaikumar, A., Kandlikar, S.G., Enhanced pool boiling for electronics cooling using porous fin tops on open microchannels with FC-78, *Applied Thermal Engineering*, Vol. 91, pp. 426-433 (2015).
[112] Collier, J.G., Thome, J.R., *Convective boiling and condensation*, Third Edition, Oxford University Press, Oxford (1994).
[113] Chen, J.C., Correlation for boiling heat transfer to saturated fluids in convective flow, *Industrial & Engineering Chemistry Process Design and Development*, Vol. 5, pp. 322-329 (1966).
[114] Mohammed Shah, M., Generalized prediction of heat transfer during subcooled boiling in annuli, *Heat Transfer Engineering*, Vol. 4, pp. 24-31 (1983).
[115] Liu, Z., Winterton, R.H.S., A general correlation for saturated and subcooled flow boiling in tubes and annuli, based on a nucleate pool boiling equation, *International Journal of Heat and Mass Transfer*, Vol. 34, pp. 2759-2766 (1991).
[116] Kandlikar, S.G., A general correlation for saturated two-phase flow boiling heat transfer inside horizontal and vertical tubes, *Journal of Heat Transfer*, Vol. 112, pp. 219-228 (1990).
[117] Thome, J.R., Cheng, L., Ribatski, G., Vales, L.F., Flow boiling of ammonia and hydrocarbons: a state-of-the-art review, *International Journal of Refrigeration*, Vol. 31, pp. 603-620 (2008).
[118] Thome, J.R., Boiling in microchannels: a review of experiment and theory, *International Journal of Heat and Fluid Flow*, Vol. 25, pp. 128-139 (2004).
[119] Kandlikar, S.G., History, advances, and challenges in liquid flow and flow boiling heat transfer in microchannels: a critical review, *Journal of Heat Transfer*, Vol. 134, pp. 034001-1 - 034001-15 (2012).
[120] Bertsch, S.S., Groll, E.A., Garimella, S.V., Review and comparative analysis of studies on saturated flow boiling in small channels, *Nanoscale and Microscale Thermophysical Engineering*, Vol. 12, pp. 187-227 (2008).
[121] Kandlikar, S.G., Grande, W.J., Evolution of microchannel flow passages-thermohydraulic performance and fabrication technology, *Heat Transfer Engineering*, Vol. 24, pp. 3-17 (2003).
[122] Kew, P.A., Cornwell, K., Correlations for the prediction of boiling heat transfer in small-diameter channels, *Applied Thermal Engineering*, Vol. 17, pp. 705-715 (1997).
[123] Ong, C.L., Thome, J.R., Macro-to-microchannel transition in two-phase flow: Part 1–Two-phase flow patterns and film thickness measurements, *Experimental Thermal and Fluid Science*, Vol. 35, pp. 37-47 (2011).
[124] Tibirica, C.B., Ribatski, G., Flow boiling in micro-scale channels–synthesized literature review, *International Journal of Refrigeration*, Vol. 36, pp. 301-324 (2013).
[125] Harirchian, T., Garimella, S.V., A comprehensive flow regime map for microchannel flow boiling with quantitative transition criteria, *International Journal of Heat and Mass Transfer*, Vol. 53, pp. 2694-2702 (2010).
[126] Kandlikar, S.G., Scale effects on flow boiling heat transfer in microchannels: A fundamental perspective, *International Journal of Thermal Sciences*, Vol. 49, pp. 1073-1085 (2010).
[127] Wang, Y., Sefiane, K., Harmand, S., Flow boiling in high-aspect ratio mini-and micro-channels with FC-72 and ethanol: Experimental results and heat transfer correlation assessments, *Experimental Thermal and Fluid Science*, Vol. 36, pp. 93-106 (2010).
[128] Hetsroni, G., Mosyak, A., Pogrebnyak, E., Segal Z., Explosive boiling of water in parallel micro-channels, *International Journal of Multiphase Flow*, Vol. 31, pp. 371–392 (2005).
[129] Wang, G., Cheng, P., Wu, H., Unstable and stable flow boiling in parallel microchannels and in a single microchannel, *International Journal of Heat and Mass Transfer*, Vol. 50, pp. 4297–4310 (2007).

[130] Bogojevic, D., Sefiane, K., Walton, A.J., Lin, H., Cummins, G., Two-phase flow instabilities in a silicon microchannels heat sink, *International Journal of Heat and Fluid Flow*, Vol. 30, pp. 854–867 (2009).
[131] Kosar, A., Kuo, C.-J., Peles, Y., Suppression of boiling flow oscillations in parallel microchannels by inlet restrictors, *Journal of Heat Transfer*, Vol. 128, p. 251-260 (2006).
[132] Kandlikar, S.G., Kuan, W.K., Willistein, D.A., Borrelli, J., Stabilization of flow boiling in microchannels using pressure drop elements and fabricated nucleation sites, *Journal of Heat Transfer*, Vol. 128, pp. 389–396 (2006).
[133] Kim, S.M., Mudawar, I., Universal approach to predicting two-phase frictional pressure drop for mini/micro-channel saturated flow boiling, *International Journal of Heat and Mass Transfer*, Vol. 58, pp. 718-734 (2013).
[134] Harirchian, T., Garimella, S.V., Microchannel size effects on local flow boiling heat transfer to a dielectric fluid, *International Journal of Heat Mass Transfer*, Vol. 51, pp. 3724–3735 (2008).
[135] Harirchian, T., Garimella, S.V., The critical role of channel cross-sectional area in microchannel flow boiling heat transfer, *International Journal of Multiphase Flow*, Vol. 35, pp. 904-913 (2009).
[136] Ma, A., Wei, J., Yuan, M., Fang, J., Enhanced flow boiling heat transfer of FC-72 on micro-pin-finned surfaces, *International Journal of Heat and Mass Transfer*, Vol. 52, pp. 2925-2931 (2009).
[137] Wei, J., Zhao, J., Yuan, M., Xue, Y., Boiling heat transfer enhancement by using micro-pin-finned surface for electronics cooling, *Microgravity Science and Technology*, Vol. 21, pp. 159-173 (2009).
[138] Guo, D., Wei, J.J., Zhang, Y.H., Enhanced flow boiling heat transfer with jet impingement on micro-pin-finned surfaces, *Applied Thermal Engineering*, Vol. 31, pp. 2042-2051 (2011).
[139] Krishnamurthy, S., Peles, Y., Flow boiling heat transfer on micro pin fins entrenched in a microchannel, *Journal of Heat Transfer*, Vol. 132, pp. 041007-1 - 041007-10 (2010).
[140] Rainey, K.N., Li, G., You, S.M., Flow boiling heat transfer from plain and microporous coated surfaces in subcooled FC-72, *Journal of Heat Transfer*, Vol. 123, pp. 918-925 (2001).
[141] Ammerman, C.N., You, S.M., Enhancing small-channel convective boiling performance using a microporous surface coating. *Journal of Heat Transfer*, Vol. 123, pp. 976-983 (2001).
[142] Sun, Y., Zhang, L., Xu, H., Zhong, X., Flow boiling enhancement of FC-72 from microporous surfaces in minichannels, *Experimental Thermal and Fluid Science*, Vol. 35, pp. 1418-1426 (2011).
[143] Bai, P., Tang, T., Tang, B., Enhanced flow boiling in parallel microchannels with metallic porous coating. *Applied Thermal Engineering*, Vol. 58, pp. 291-297 (2013).
[144] Kim, D.W., Bar-Cohen, A., and Han, B. Forced convection and flow boiling of a dielectric liquid in a foam-filled channel, 2008 11*th Intersociety Conference on Thermal and Thermomechanical Phenomena in Electronic Systems*, ITHERM 2008, 28-31 May, Orlando, USA (2008).
[145] Lu, W., Zhao, C.Y., Numerical modelling of flow boiling heat transfer in horizontal metal-foam tubes, *Advanced Engineering Materials*, Vol. 11, pp. 832-836 (2009).
[146] Pranoto, I., Leong, K.C., An experimental study of flow boiling heat transfer from porous foam structures in a channel, *Applied Thermal Engineering*, Vol. 70, pp. 100-114 (2014).
[147] Li, H.Y., Leong, K.C., Experimental and numerical study of single and two-phase flow and heat transfer in aluminum foams, *International Journal of Heat and Mass Transfer*, Vol. 54, pp. 4904-4912 (2011).
[148] Madani, B., Tadrist, L., Topin, F., Experimental analysis of upward flow boiling heat transfer in a channel provided with copper metallic foam, *Applied Thermal Engineering*, Vol. 52, pp. 336-344 (2013).
[149] Gungor, K.E., Winterton, R.H.S., Simplified general correlation for saturated flow boiling and comparisons of correlations with data, *Chemical Engineering Research and Design*, Vol. 65, pp. 148-165 (1987).

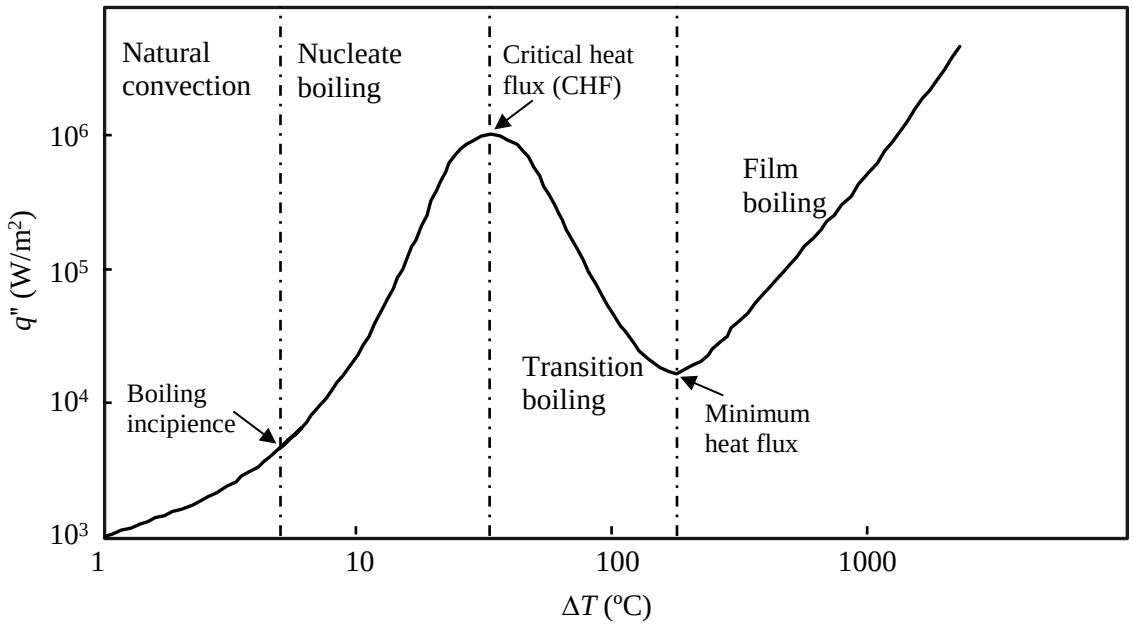

Fig. 1 Illustration of Nukiyama boiling curve.

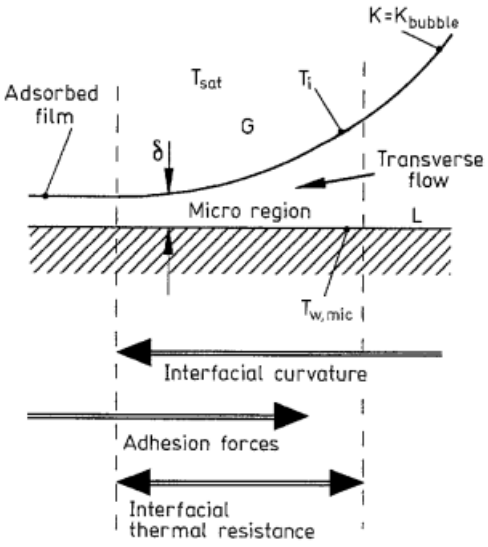

Fig. 2 Illustration of three-phase contact line [23].

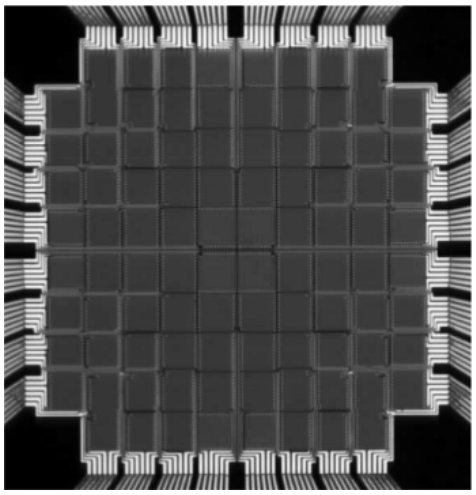

Fig. 3 Photograph of micro-heaters array with each heater nominally 0.1 mm^2 in area [34].

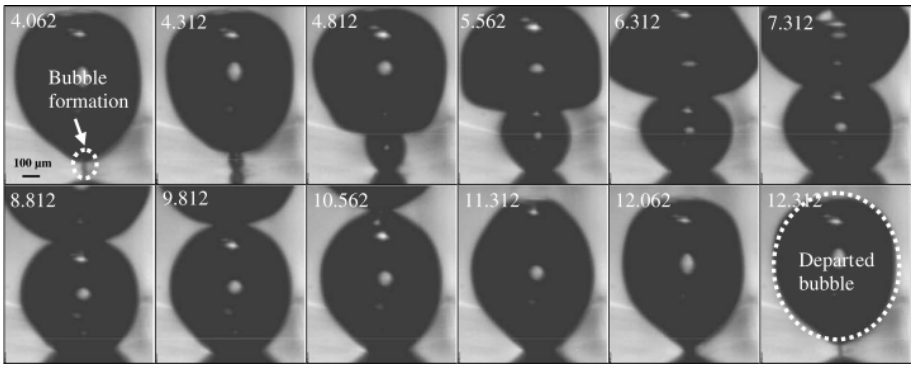

Fig. 4 Bubble ebullition cycle in millisecond time scale and 100 μm length scale [37].

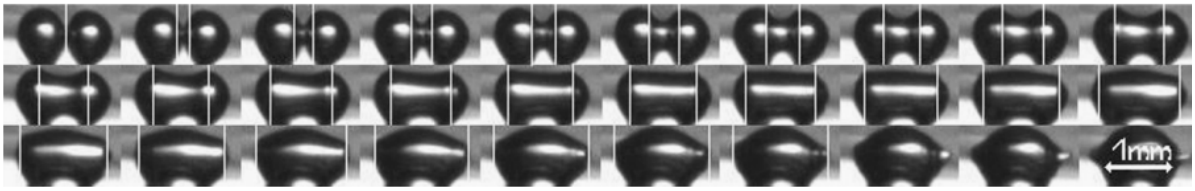

Fig. 5 Wave-front propagation (indicated in vertical white line) during lateral bubble coalescence [40].

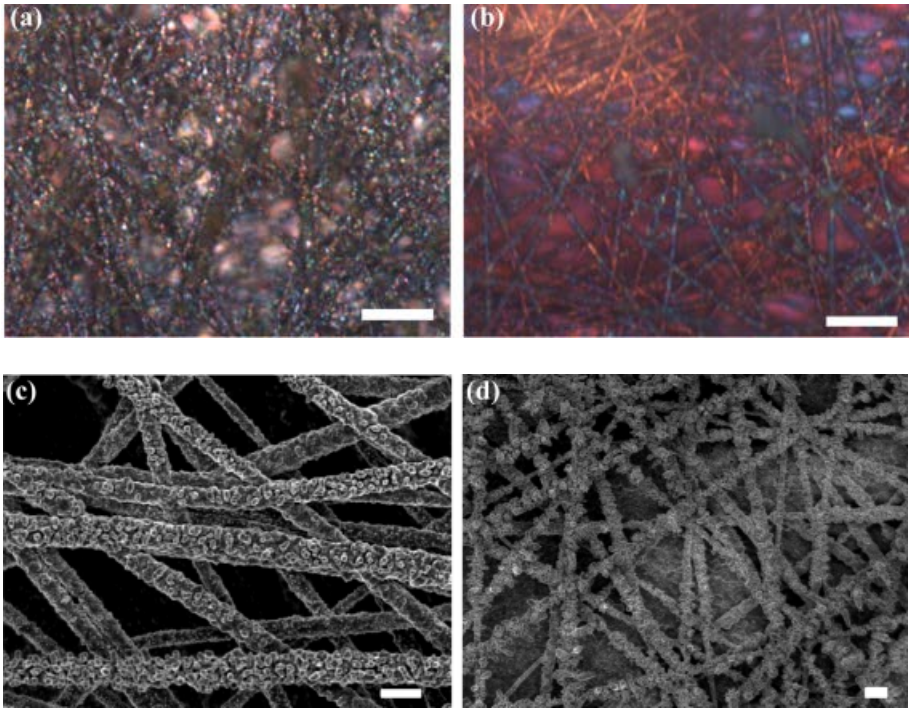

Fig. 6 Microscope images at 10 µm scale (a, b) and SEM images at 1 µm (c, d) of copper-plated nanofiber [69].

Fig. 7 Photographs of surface produced by particle sintering with particle size of 850-1000 μm (a) top view (b) side view [73].

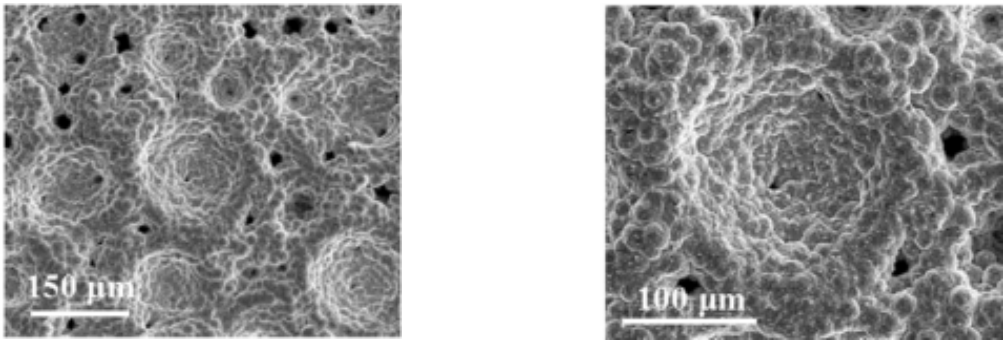

(a) (b)

Fig. 8 SEM images of microporous surface at (a) 150 µm and (b) 100 µm scales [78].

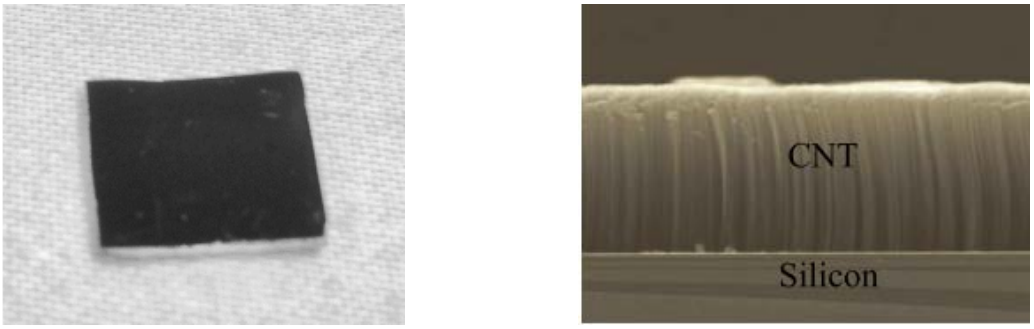

(a) (b)

Fig. 9 (a) Photographs of fully coated CNT surface produced by CVD (b) SEM image of vertically-aligned CNT array [50].

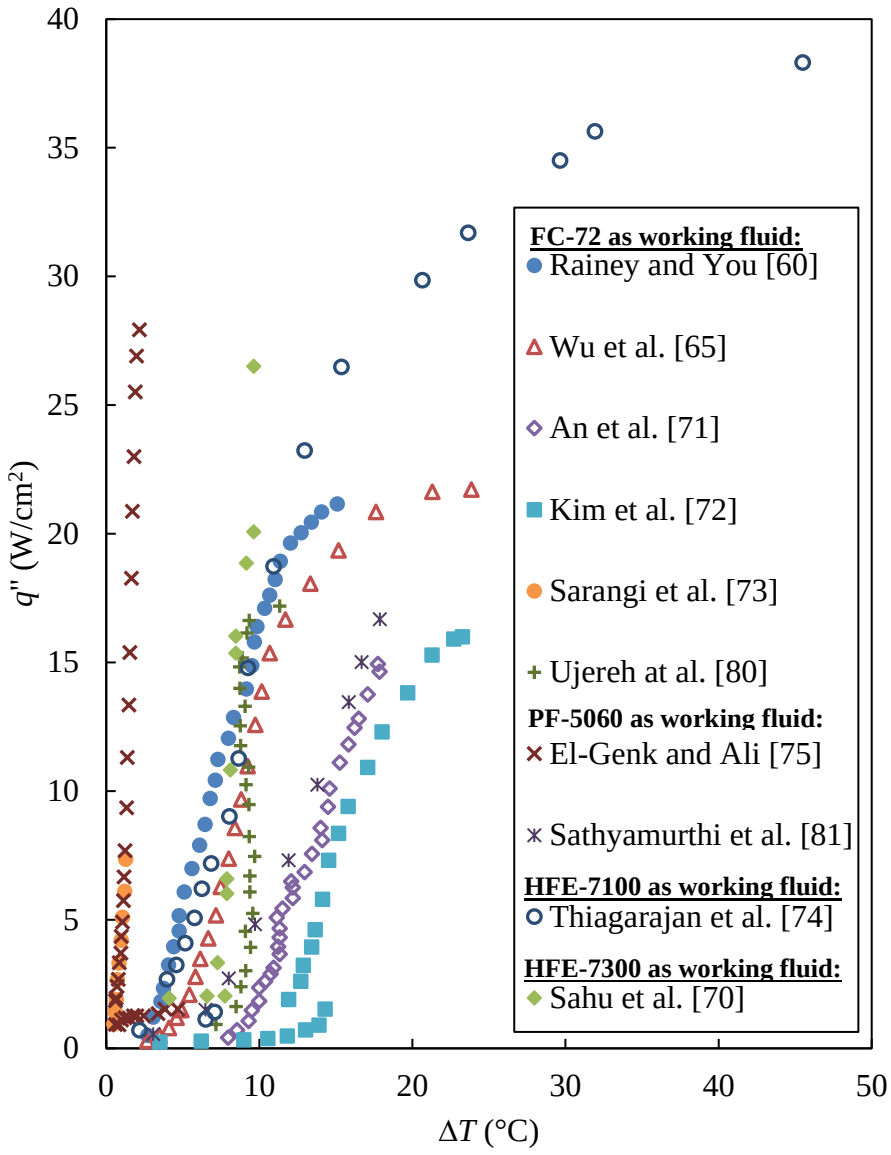

Fig. 10 Comparison of pool boiling curves of the better performing coated surfaces reproduced from selected publications.

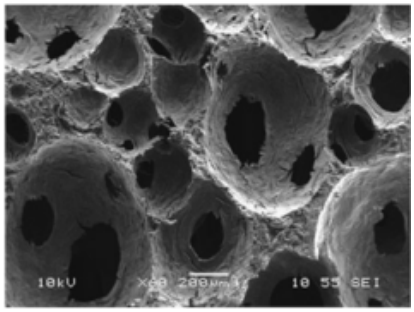

(a)

(b)

Fig. 11 (a) Scanning electron microscope images of graphite foam internal structure [98] (b) finned porous graphite [99].

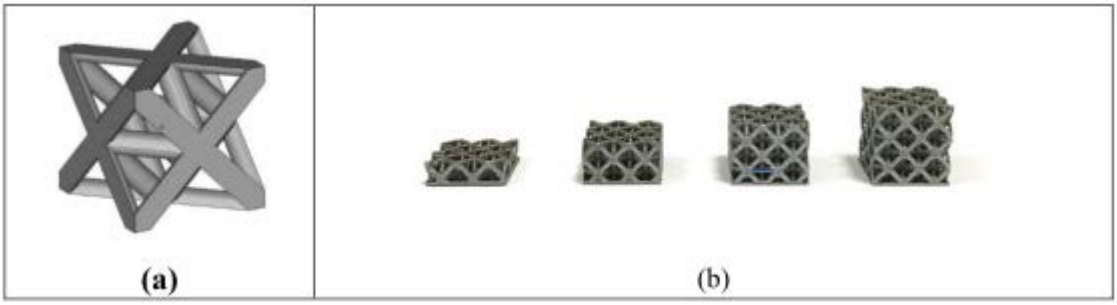

Fig. 12 (a) Unit of Octet-truss and (b) porous structures of height range 2.5 mm to 10 mm fabricated by Wong et al. [107].

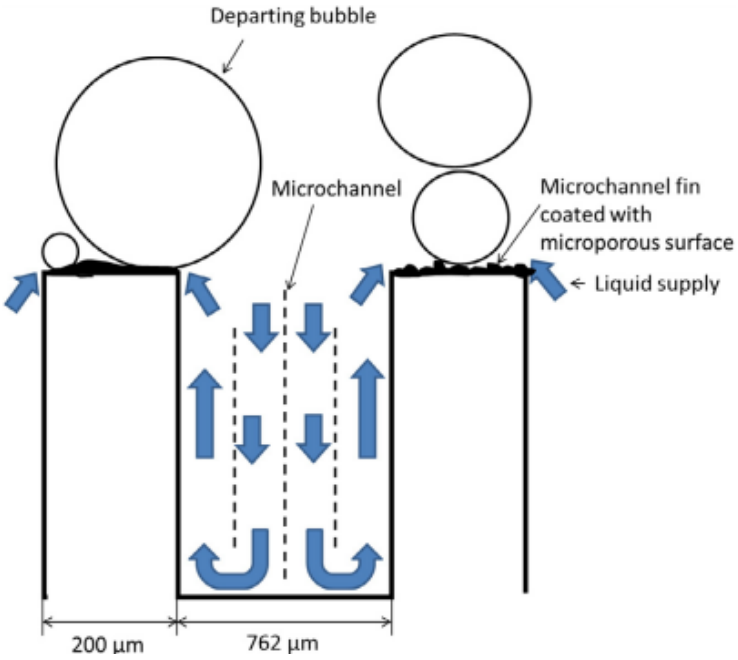

Fig. 13 Liquid-vapor pathways on a hybrid surface as proposed by Patil and Kandlikar [110].

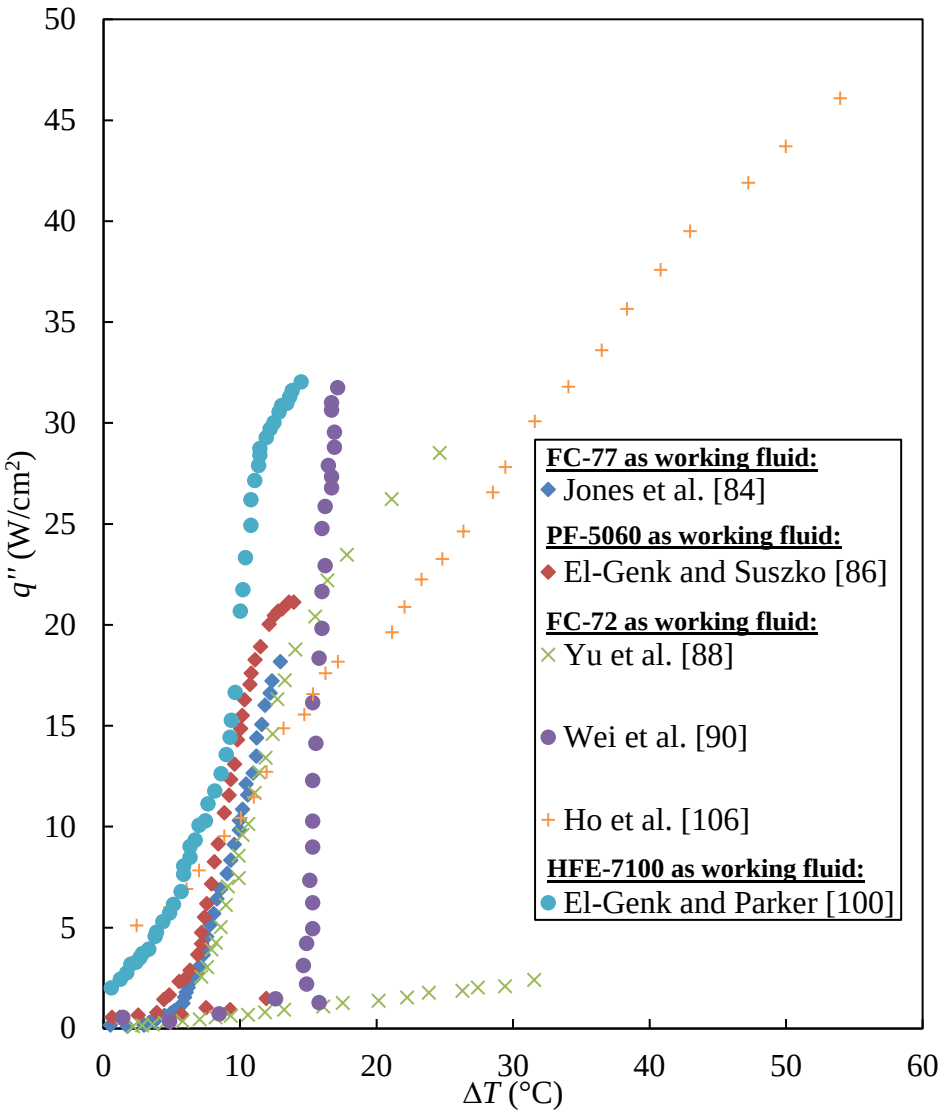

Fig. 14 Comparison of pool boiling curves of the better performing intrinsic surfaces reproduced from selected publications.

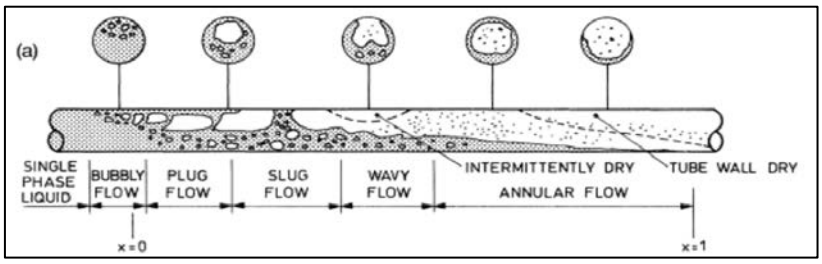

Fig. 15 Illustration of flow boiling regimes [112].

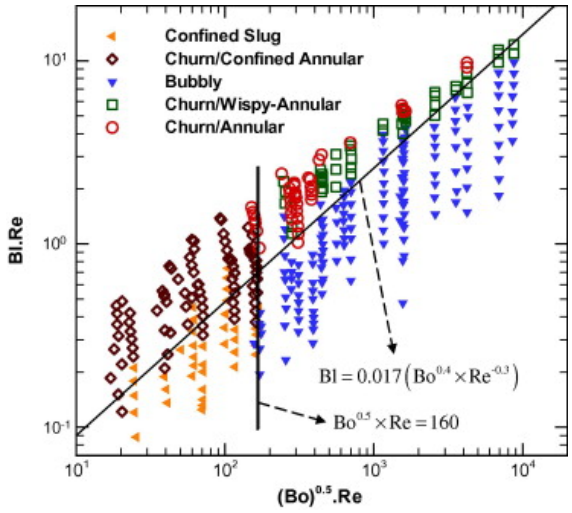

Fig. 16 Comprehensive flow regime map for FC-77 [125].

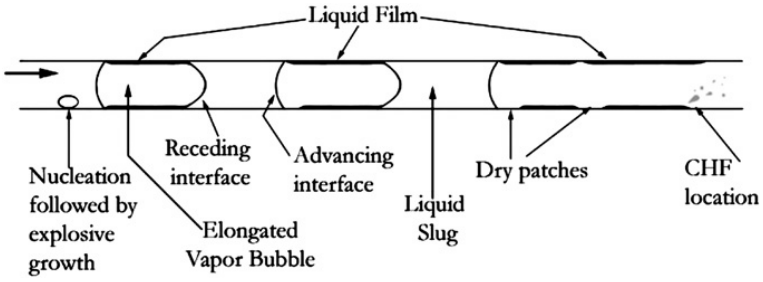

Fig. 17 Representation of different heat transfer mechanisms during elongated bubble/slug flow patterns [126].

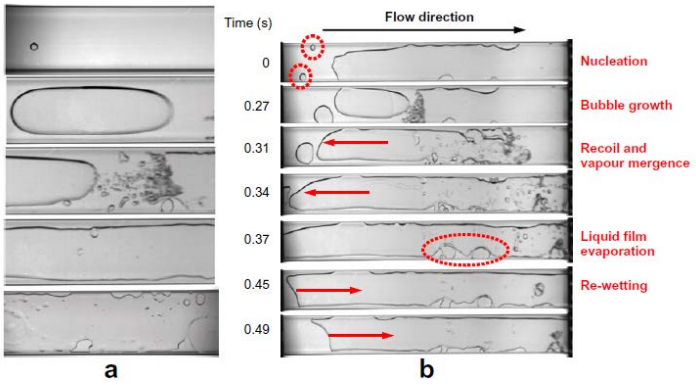

Fig. 18 Flow regimes of FC-72 boiling in the channel with d_h = 1454 µm, (a) slug and annular flow, camera speed: 1500 fps, (b) wispy-annular flow at G = 22.4 kg/m^2·s and q'' = 8.13 kW/m^2, camera speed: 1000 fps [127].

Table 1 Thermophysical properties of dielectric fluids [13] and water at 1 atm and 25°C

	FC-72	FC-87	HFE-7000	HFE-7100	HFE-7300	Water
Boiling point (°C)	56	30	34	61	98	100
Liquid density (kg/m^3)	1680	1650	1400	1510	1660	997
Liquid dynamic viscosity (kg/m·s)	6.4×10^{-4}	4.5×10^{-4}	4.5×10^{-4}	5.8×10^{-4}	11.8×10^{-4}	8.9×10^{-4}
Liquid specific heat (J/kg·K)	1100	1100	1300	1183	1140	4182
Liquid thermal conductivity (W/m·K)	0.057	0.056	0.075	0.069	0.063	0.61
Latent heat of vaporization (kJ/kg)	88	103	142	112	102	2257
Liquid surface tension (mN/m)	10.0	9.0	12.4	13.6	15.0	72.0

Table 2 Summary of pool boiling with coated surfaces

Reference	Surfaces characteristics	Test conditions	Working fluids	Nucleate boiling performances in comparison with plain/ reference surfaces
Epoxy binding				
Rainey and You [60]	- Diamond particles of 8-12 µm in size coated onto copper substrate.	- Pool boiling at atmospheric pressure - Boiling surface dimensions of 2 × 2 and 5 × 5 cm - Boiling surface orientation 0º-180º	FC-72	- More than 300% enhancement in *h* at 0° surface orientation - 64% enhancement in CHF (or 21.7W/cm^2) at 0° surface orientation
Arik et al. [63]	-Diamond particles of 8-12 µm in size coated onto copper substrate. - Coating thickness of 50-75 µm.	- Saturated and 0-72 K subcooled pool boiling - System pressure ranged from 101.3 kPa to 303.9 kPa	FC-72	- 60% enhancement in CHF (or 47 W/cm^2)
Dipping and dripping process				
Wu et al. [65]	- TiO_2 coated onto smooth copper surface, 1 µm thick and average roughness of 1.55 µm. - SiO_2 coated onto smooth copper surface, 1 µm thick and average roughness of 1.41µm.	- Pool boiling at atmospheric pressure	FC-72 and water	- Max. 91.2% enhancement in *h* with FC-72 - Max. 38.2% enhancement in CHF (or 22.8W/cm^2) with FC-72
Spray coating				
Sahu et al. [70]	- Copper plated nanofiber of 15-20 µm coated onto copper substrate.	- Saturated pool boiling	HFE-7300 and water-heptanol mixtures	- Max. 33% enhancement in CHF (or ≈ 26 W/cm^2)

An et al. [71]	- Reduced graphene oxide (rGO) coated onto copper substrate. - Coating resulted in average roughness of 495 nm.	- Pool boiling at 0.24 bar and 20°C bulk fluid temperature	FC-72	- Max. 1.5 times enhancement in *h* (or 8.5 kW/m^2·K) - Max. 0.5 times enhancement in CHF (or 149.6 kW/m^2)

Free particle and particle sintering

Kim et al. [72]	-Copper free particles of sizes ranging from 20 nm - 9 mm placed on polished copper surface.	- Pool boiling at atmospheric pressure	FC-72	- Max. 76.3% enhancement in average *h* - Max. 10% enhancement in CHF (or 160 kW/m^2)
Sarangi et al. [73]	-Copper free and sintered particles of sizes ranging from 45 - 1000 µm coated onto polished copper surface.	- Pool boiling at atmospheric pressure	FC-72	-Free particles: 32% reduction in wall superheat; 44% higher CHF (or 161 kW/m^2) -Sintered particles: 95% reduction in wall superheat; 33% reduction in CHF
Thiagarajan et al. [74]	- Copper-rich microparticles diameters 5 - 20 µm. - Coating thickness 100 µm, 360 µm and 700 µm on plain copper surface.	- Saturated pool boiling at atmospheric pressure	HFE-7100	-Max. 270% enhancement in *h* -Max. 60% enhancement in CHF (or ≈ 45 W/cm^2)

Electrochemical deposition

El-Genk and Ali [75]	- Micro-porous layers of thickness 95, 139, 171, 197 and 220 µm coated onto copper substrate. - Pore diameter 30 - 60 µm	- Saturated pool boiling at atmospheric pressure	PF-5060	- More than 17 times enhancement in max. *h* (or 13.5 W/m^2·K) - Max. 70% enhancement in CHF (or 27.8 W/cm^2)
Ali and El-Genk [78]	- Micro-porous layers of thickness 80 and 137 µm coated onto copper substrate.	- Saturated pool boiling at atmospheric pressure - Boiling surface orientation 0º-180º	PF-5060	- 9.5 times (or 4.2 W/cm2) enhancement in max. *h* at 180º surface orientation - Max. 87% enhancement in CHF (or 8.6 W/cm^2) at 180º surface orientation
Furberg and Palm [79]	- Porous layer of thickness 250 µm coated onto copper surface. - Consist of pores with average diameter 105 µm and dendritically shaped structures with 0.1-1 µm cavities.	- Saturated pool boiling - 0.7 bar, 45.8°C saturation temperature for FC-72 - 5 bar, 15.7°C saturation temperature for R134a	FC-72 and R134a	- Approximately 5 times higher in *h* for boiling with FC-72

Chemical vapor deposition

Ujereh et al. [80]	- MWCNT diameter 50 nm; height 20 - 30 µm. - Fully light and dense array CNT coated on silicon substrate. - Patterned 'grid' and 'island' array CNT coated on silicon substrate. - Fully coated CNT on copper and copper microstud substrate.	- Saturated pool boiling at atmospheric pressure	FC-72	- Max. 452% enhancement in *h* (or 18,200 W/m^2·K) - Max. 44.8% enhancement in CHF (or 18.1 W/cm^2)

Sathyamurthi et al. [81]	- MWCNT diameter 8 - 15nm; height 9 and 25 µm. - CNT coated on atomically smooth bare silicon substrate.	- Saturated and 5 - 30 ºC subcooled pool boiling at atmospheric pressure	PF-5060	- CNT coated surface 64.6% increase in heat flux at same wall superheat as compared to bare silicon. - Up to 62% enhancement in CHF (or 18.4 W/cm^2)
Ho et al. [50]	- MWCNT diameter 10 nm; height 215 µm. - Fully coated and interlaced patterned coated CNT surfaces on silicon substrate.	-Saturated pool boiling at atmospheric pressure - Boiling surface orientation 0º - 180º	FC-72	- Max. 86% enhancement in average *h* (or 0.45 W/cm^2·K) - Max. 42% enhancement in CHF (or 20.1 W/cm^2)

Table 3 Summary of pool boiling with intrinsic surfaces

Reference	Surfaces characteristics	Test conditions	Working fluids
Electrical discharge machining (EDM)			
Guglielmini et al. [82]	- Array of copper pin fins with square cross-section. - Pin fin width 0.4 to 1.0 mm. - Pin fin length 3 and 6 mm. - Pin fin spacing 1.2 and 3.0 mm.	- Saturated pool boiling at 0.5, 1.0 and 2.0 bar	FC-72
Yu and Lu [83]	- Array of copper pin fins with square cross-section. - Pin fin width 1.0 mm. - Pin fin length 0.5, 1.0, 2.0 and 4.0 mm. - Pin fin spacing 0.5, 1.0 and 2.0 mm.	- Saturated pool boiling at atmospheric pressure	FC-72
Jones et al. [84]	- Roughened surfaces with averaged surface roughness of 1.08, 2.22, 5.89 and 10.00 μm.	- Saturated pool boiling at atmospheric pressure	FC-77 and water
Mechanically roughened surfaces			
El-Genk and Suszko [86] and Suszko and El-Genk [87]	- Roughened surfaces with average surface roughness ranging from 0.039 to 1.79 μm.	- Saturated pool boiling at atmospheric pressure - Boiling surface orientation 0º-180º	PF-5060
Micro/nano-electro-mechanical (MEMS/ NEMS) processes			
Yu et al. [88]	- Cylindrical cavity arrays - Cavity diameters 50, 100 and 200 μm - Cavity depth 110 and 200 μm - Cavity spacing 100, 200 and 400 μm	- Saturated pool boiling at atmospheric pressure	FC-72
Wei et al. [90]	- Micro-pin-fins arrays - Fin width 30 μm - Fin height 60 and 200 μm	- Saturated and 3-45 K subcooled pool boiling at atmospheric pressure - Degassed and gas dissolved	FC-72

Xue et al. [91] and Zhang et al. [92]	- Micro-pin-fins arrays - Fin width 30 and 50 µm - Fin height 60 and 120 µm	- 31.3-44.5 K subcooled pool boiling atmospheric pressure - Microgravity environment	FC-72

Open cell foams

Leong et al. [97] and Pranoto et al. [99]	- Block and finned "Kfoam" graphite foams of 78% volume porosity and 0.5 mm pore diameter. - Block and finned "Pocofoam" graphite foams of 61-75% porosity and 0.31-0.35 mm pore diameter.	- Saturated pool boiling	FC-72 and HFE-7000
El-Genk and Parker [100]	- Porous graphite of 60% volume porosity. - Consist of pore and re-entrant cavities of a few to hundreds of micrometers in size.	- Saturated and 10-30 K subcooled pool boiling at atmospheric pressure	HFE-7100

Selective laser melting (SLM)

Ho et al. [106]	- Surfaces with array of microcavities (500 and 700 µm cavity mouth diameter). - Surfaces with array of microfins (350 and 500 µm fin diameter).	- Pool boiling at atmospheric pressure	FC-72
Wong and Leong [107]	- Octet-truss porous structures of 70% volume porosity and 2.5-10 mm height.	- Pool boiling at atmospheric pressure	FC-72

Table 4 Summary of flow boiling with enhanced surfaces

Reference	Surfaces characteristics	Test conditions	Working fluids
Intrinsic surfaces			
Ma et al. [136]	- Micro-pin-fins arrays - Fin width 30 µm - Fin height 60 and 120 µm	- Fluid velocities of 0.5, 1 and 2 m/s - 15, 25 and 35 K liquid subcooling	FC-72
Wei et al. [137]	- Micro-pin-fins arrays - Fin width 30 and 50 µm - Fin height 60 and 120 µm	- Fluid velocities of 0.5, 1 and 2 m/s - 15, 25 and 35 K liquid subcooling	FC-72
Guo et al. [138]	- Micro-pin-fins arrays - Fin width 30 and 50 µm - Fin height 60 and 120 µm	- Fluid velocities of 0.5, 1 and 1.5 m/s - Jet impingement velocities of 0, 1 and 2 m/s - 25 and 35 K liquid subcooling	
Krishnamurthy and Peles [139]	- Pin fins 100 µm width - Microchannel with hydraulic diameter of 222 µm - 24 pin fins in a microchannel	- Mass fluxes of 350 to 827 kg/m^2·s	HFE-7000
Porous coated surfaces			
Rainey et al. [140]	- ABM microporous coating of about 0.1–1 mm size cavities that is approximately 50 mm thick	- Fluid velocities of 0.5, 2 and 4 m/s - 4, 10 and 20 K liquid subcooling	FC-72
Ammerman and You [141]	- Square minichannel of 2 mm side length and heated length of 8 cm - Microporous coating of diamond powder with 8 – 12 µm particle size	- Mass fluxes of 500, 2000 and 5000 kg/m^2·s - 2 to 21 K liquid subcooling	FC-87
Sun et al. [142]	- Horizontal, rectangular minichannels of 0.49, 0.93 and 1.26 mm hydraulic diameter	- Mass flux of 700 kg/m^2·s - 20 K liquid subcooling	FC-72

	- Microporous coating of sintered copper particles of 20, 50 and 120 μm diameters		
Bai et al. [143]	- Fifteen parallel microchannels of 400 mm in width, 900 mm in depth and 32 mm in length - Microporous coating of dendrite copper powders with diameters of about 30, 55 and 90 mm	- Mass flux of 182.8 kg/m^2·s - 58 K liquid subcooling	Anhydrous ethanol
Porous foams			
Kim et al. [144]	- Heated channel of 10 mm width, 7 mm height and 37 mm length - Copper foams of 10 and 20 PPI, porosities of 92% and 95%	- Mass fluxes of 20, 48 and 72 kg/m^2·s	FC-72 and water
Pranoto and Leong [146]	- Graphite foams of porosities of 61% and 72% - Foam dimension of 80 mm length, 60 mm width and 6mm height	- Mass fluxes of 50, 100 and 150 kg/m^2·s	FC-72
Madani et al. [148]	- Upward flow channel of 50 mm length, 10 mm width and 100 mm height - Copper foam of 36 PPI and porosity of 97%	- Mass fluxes of 6, 38, 57 and 76 kg/m^2·s	n-pentane